Evolution of lateralized gustation in nematodes

Marisa Mackie[1], Vivian Vy Le[1], Heather R. Carstensen[1], Nicole R. Kushnir[1], Dylan L. Castro[1], Ivan M. Dimov[1], Kathleen T. Quach[2], Steven J. Cook[3,4], Oliver Hobert[3], Sreekanth H. Chalasani[2], and Ray L. Hong[1,*]

[1] Department of Biology
California State University,
Northridge, CA, USA

[2] Molecular Neurobiology Laboratory
Salk Institute for Biological Studies,
La Jolla, CA, USA

[3] Department of Biological Sciences
Howard Hughes Medical Institute,
Columbia University,
New York, NY, USA

[4] Present address:
Neural Coding Department
Allen Institute for Brain Science,
Seattle, WA, USA

***Corresponding author:** ray.hong@csun.edu

Animals with small nervous systems have evolved left and right asymmetry in their neurons to process various salts at different concentrations.

Keywords: calcium imaging, lateral asymmetry, chemosensory neurons, *Pristionchus pacificus*

Abstract:

Animals with small nervous systems have a limited number of sensory neurons that must encode information from a changing environment. This problem is particularly exacerbated in nematodes that populate a wide variety of distinct ecological niches but only have a few sensory neurons available to encode multiple modalities. How does sensory diversity prevail within this constraint in neuron number? To identify the genetic basis for patterning different nervous systems, we demonstrate that sensory neurons in *Pristionchus pacificus* respond to various salt sensory cues in a manner that is partially distinct from that of the distantly related nematode *Caenorhabditis elegans*. By visualizing neuronal activity patterns, we show that contrary to previous expectations based on its genome sequence, the salt responses of *P. pacificus* are encoded in a left/right asymmetric manner in the bilateral ASE neuron pair. Our study illustrates patterns of evolutionary stability and change in the gustatory system of nematodes.

Introduction:

Nematodes form a vast array of ecological relationships, from specialized parasite-host dependencies to nematode-microbial interactions, each one demanding exquisitely fine-tuned sets of sensory palates that span multiple modalities (*1–8*). Yet, the number of sensory neurons across diverse nematode species seems to be constrained (*9–11*). Several free-living and parasitic nematode species examined by serial section electron microscopy have nearly identical numbers of 12-13 pairs of head sensory neurons, known as the amphid neurons (*11–15*). How does sensory diversity arise within this constraint in neuron number? When coupled with well-described neuronal anatomy, this conserved neuron count allows for detailed comparisons at the single-cell resolution and represents an opportunity to interrogate how sensory cues are processed by anatomically similar nervous systems to produce species-specific or developmental stage-dependent behavioral outputs. To identify the genetic basis for patterning different nervous systems and to understand the processes that underlie evolutionary changes in adapting to different environments, several comparative model systems have been developed to promote comparisons to the well-studied nematode *Caenorhabditis elegans* at the genetic and cellular levels, including the predatory entomophilic nematode, *Pristionchus pacificus* (*11*, *16–19*).

As expected from their association with insects in the wild, the olfactory preferences of *P. pacificus* are distinct from those of *C. elegans* and the human parasite *Strongyloides stercoralis* (*2*, *3*, *20*), but little is known about *P. pacificus* responses to water-soluble compounds. In *C. elegans,* the main salt receptor neuron class comprises of a bilateral pair of left and right ASE neurons (ASEL and ASER), which serve to induce an attractive locomotory response toward an increase in salt concentration (*21*). The gene *che-1* (*che*mosensory defective) encodes a transcription factor that is exclusively expressed in the ASE neurons and is required for their proper differentiation, such that a *che-1* mutant results in defective salt attraction (*22–25*).

One major role of *C. elegans* CHE-1 is to promote lateral asymmetry in the ASE neurons. The left and right ASE neurons asymmetrically express receptor-type guanylyl cylases (rGCs, encoded by *gcy* genes) (*26*). This finding led to the realization that the ASE neurons are lateralized, such that the left and the right ASE neurons differentially

respond to distinct salt ions (*27–30*). This observation led in turn to the identification of a complex gene regulatory network that genetically programs the distinct sensory potentials of the left and right ASE neurons (*31*), which includes a miRNA, *lsy*-6, at the top of this gene regulatory network (*31–33*). However, the *lsy-6* miRNA evolved selectively in the *Caenorhabditis* genus (*34*) and is absent in *P. pacificus.* Moreover, *P. pacificus* does not show an expansion of the ASEL-type and ASER-type rGCs, as *C. elegans* does (*11*) . With these two genomic observations in mind, we had previously proposed that the ASE neurons are unlikely to be lateralized in *P. pacificus* (*11*).

However, we now revise this view in light of our work on mapping chemosensory responses in *P. pacificus* on the level of behavior and neuronal activity. We demonstrate that *P. pacificus* does in fact show lateralized chemosensory profiles, indicating that *P. pacificus* must have evolved independent means to establish ASE laterality. We also show that the tastant palate of *P. pacificus* is distinct from that of *C. elegans*, and that its dependence on ASE, as well as its terminal selector transcription factor *che-1*, have also diverged.

Results

P. pacificus and C. elegans differ in their behavioral responses to salts

Previous cross-species comparisons between *P. pacificus* and *C. elegans* indicated strong differences in olfaction preferences that reflect their divergent evolutionary histories and ecology (*2*). To identify the neurons that mediate gustation, we first compared the chemosensory profiles of these two species toward water-soluble ions. In this survey, we found ammonium salts to be the strongest attractants to wildtype *P. pacificus* J4 to adult hermaphrodites (NH_4Br, NH_4Cl, NH_4I), with NH_4I significantly more attractive to *P. pacificus* compared to *C. elegans* (Fig. 1). Notably, in contrast to *C. elegans* (*35*), we find that *P. pacificus* is less attracted to NaCl and LiCl compared to the ammonium salts (Fig. 1). Also, *P. pacificus* is repulsed by acetate salts (NaAc, NH_4Ac), which induce attractive responses in *C. elegans* (*36*). We conclude that *P. pacificus* and *C. elegans* display differences in their salt preferences.

Ppa-che-1 shows similarities and difference to *Cel-che-1* in both expression and function

The *C. elegans che-1* mutant (*che*motaxis-defective) was originally isolated for its inability to respond to a broad panel of salt tastants (*22*, *35*), including those described above (*29*, *30*, *36*). *che-1* was found to encode for a Zn finger transcription factor that is exclusively expressed in the ASE neuron pair (*25*), which through laser ablations had been found to be the main salt receptor neurons (*37*). *che-1* was found to control the entire differentiation of the ASE neurons, including the expression of putative receptors of the GCY receptor guanylyl cyclase family (*23–25*, *38*).

To assess whether *che-1* performs a similar function in salt perception for *P. pacificus* as for *C. elegans,* we analyzed the expression and function of the *Ppa-che-1* ortholog. In a previous paper, we reported that the 5' region of the sole *Pristionchus che-1* ortholog directs reporter expression to the *Ppa* ASE and *Ppa* ASG neuron classes (*11*). Re-examination of our provisional cell identifications using a newly-generated *che-1p::GFP* strain with stronger neurite expression revealed highly elaborated finger-like dendritic endings in the more anterior amphid neuron that could unambiguously be

assigned to the AFD neurons (Fig. 2A-C), prompting us to reassign expression of *che-1* to ASE and AFD.

We confirmed that the *che-1* reporter transgene indicates the full expression of the endogenous *che-1* locus by tagging the endogenous *che-1* locus with an ALFA-tag (*39*). The *che-1::ALFA* animals showed staining in 2 pairs of head neurons whose position is consistent with being the ASE and AFD neurons (Fig. 2D-E). By crossing the *che-1* reporter transgene into a *che-1* mutant background (see below), we also found that *che-1* autoregulates its own expression especially in the ASE neurons (Fig. 2F, GFP expression in 97% in WT (n= 36) vs 4% in *che-1(-)*(n=48)), as it does in *C. elegans* (*25*). The reduction of *che-1p::GFP* in the AFDs was also observed (GFP expression in 100% in WT (n= 36) vs 33% in *che-1(-)*(n=48)).

To provide further evidence that *Ppa*-CHE-1 is indeed expressed in the *Ppa*-AFD neurons, we analyzed the expression of the *Ppa-ttx-1p::RFP* reporter. In *C. elegans*, the OTX homeodomain transcription factor TTX-1 is a terminal selector expressed in the AFD neurons required for designating the AFD fate (Satterley 2001). We found *ttx-1p::GFP* to be strongly expressed in a pair of neurons with the hallmark finger-like dendritic ending of the AFD neurons (Fig. 2G-H), as well as expression in other head and tail neurons (possibly RIP and RIB) and cells likely to be the pharyngeal marginal cells based on likely conservation with *Cel-ttx-1* expression (Reilly 2022). To confirm that endogenous TTX-1 protein expression is co-expressed with *che-1p::GFP*, we examined C-terminally tagged *ttx-1:ALFA* animals and found co-localization in the same anterior pair of amphid neurons, but no co-expression in the posterior pair of amphid neurons (Fig. 2I-J, n=15). Interestingly, the promoter expression in the posterior pair of amphid neurons in animals with both *ttx-1p::RFP* and *gcy-22.3p::GFP* reporters do co-localize in the ASER neurons (Fig. S1), possibly due to differences between the expression patterns of the 4 possible *ttx-1* splice forms. The transcriptional and protein co-expression of *ttx-1* and *che-1* in the AFD neurons unequivocally show the expression of *che-1* in both AFD and ASE neurons in *P. pacificus.*

Next, we examined whether *P. pacificus* salt responsiveness shows similar *che-1* dependence as in *C. elegans*. We generated two putative null alleles in the *Ppa-che-1* homolog using CRISPR/Cas9 genome engineering, through introduction of small

deletions in the first exon of the gene, thereby resulting in frameshift and premature stops (Fig. 3A). Both *Ppa-che-1* alleles exhibited defects in attraction towards NH_4Cl and LiCl compared to wildtype (Fig. 3B). However, unlike in *C. elegans*, *Ppa-che-1* mutants showed no detectable difference in responses to NH_4I, NaCl, and NaAc.

We considered two different possibilities for the behavioral differences of *Ppa-che-1* and *Cel-che-1* mutants. *P. pacificus* may use sensory neurons other than ASE to sense these cues, or alternatively, *Ppa-che-1* may not have the same fundamental impact on ASE function in *P. pacificus* as it does in *C. elegans.* To explore these different possibilities, we silenced *che-1* expressing neurons by expressing codon-optimized HisCl1 channel under control of the *che-1* promoter. Histamine-treated *che-1p::HisCl1* animals showed complete loss of attraction to NH_4Br, NH_4Cl, and NH_4I but did not significantly alter their repulsive response to NaAc (Fig. 3C). As a control, we show that the presence of the *che-1p::HisCl1* transgene was necessary for the knockdown of NH_4Br attraction (Fig. S2). These findings corroborate that NaAc is sensed by neurons other than ASE (or AFD, in which the *che-1* promoter also drives HisCl1). Since NH_4I sensation is affected by silencing of *che-1(+)* neurons but is unaffected in *che-1* mutants, ASE function may be more greatly impacted by the silencing of ASE than by the loss of *che-1*.

The ASE neurons show left/right asymmetric responses to salt

To assess whether *Ppa* ASE neurons show the same lateralized response to salt ions as *Cel* ASE neurons, we generated transgenic *P. pacificus* lines that express RCaMP in ASE neurons and assessed calcium responses to attractive salts (Fig. 4, S3-S4). Specifically, we looked for changes in calcium levels immediately after the addition and removal of specific salts. When 250 mM NH_4Cl is administered, an ‘ON’ response is observed as calcium transiently increases in the left ASE neuron (ASEL). In contrast, an ‘OFF’ response was observed as calcium sharply dips in the right ASE neuron (ASER) before quickly returning to baseline when the salt was removed, which suggests hyperpolarization of this neuron (Fig. 4A-B)(*29*). However, when presented with a 10-fold lower concentration of 25 mM NH_4Cl, the ‘OFF’ response completely disappeared in ASER while the ‘ON’ response became more pronounced in ASEL. The ASER responses to 250 mM and 25 mM NaCl (Fig. 4D) were very similar to the ‘OFF’ response (including

hyperpolarization) observed for NH_4Cl, but the ASEL responses differ between the two salts: instead of the 'ON' response expected of ASEL, we observed a relatively weak 'OFF' response without the characteristic hyperpolarization but accompanied by an attenuated 'bump', a profile that we classify as an 'OFF-2' response (Fig. 4C). Finally, we examined the response to NH_4I and found that it also elicited laterally asymmetric responses, but yet again distinct from the responses to both NH_4Cl and NaCl, with ASEL showing a strong 'ON' response, and ASER showing an 'ON-OFF' biphasic response to 250 mM NH_4I (Fig. 4E-F)(*40*, *41*). Interestingly, the ASER exhibited an 'OFF'-only response to 25 mM NH_4I, which was not observed for the same concentration of NH_4Cl and NaCl, and thus may reflect the higher response to NH_4I than to NH_4Cl and NaCl in the behavior assays. Altogether, *P. pacificus* ASE neurons clearly show left/right asymmetric responses to salt attractants and these asymmetric responses show similarities and differences to the *C. elegans* ASE taste neurons (see Discussion).

The AFD neurons also respond to salts in *P. pacificus*

The RCaMP line that we used to assess calcium responses in ASE is also expressed in AFD, allowing us to simultaneously examine the calcium responses in the AFD (AM12) neurons (Fig. 5, S1, S5-S7). Surprisingly, we detected a distinctly 'ON-OFF' biphasic response to all 3 salt types at both concentrations. Specifically, although we observed weaker or comparable responses in AFD neurons when compared to either ASE neuron's response towards 250 mM NH_4Cl, NaCl and NH_4I (Fig. 5A-B, 5E-F, 5I-J), the AFD responses were more robust than ASER toward 25 mM NH_4Cl, NaCl, and NH_4I (Fig. 5D, 5H, 5L). Specifically, AFD neurons responded strongly to 25 mM NaCl when neither one of the ASE neurons showed a positive response (Fig. 5G-H). Averaging the calcium transients separately by AFD left versus right did not result in significant differences in the shape of the neuronal calcium responses, with the exception of the AFDR responses to higher versus lower concentrations of NH_4I (Fig. S6-S7). We have not further pursued whether these AFD responses are a reflection of a direct perception of salt or a secondary consequence of communication of salt-perceptive neurons (like ASE) to AFD.

A target of *che-1*, the guanylyl cyclase *gcy-22.3* is required for chemotaxis

We further explored the asymmetric salt perception by the ASE neurons, which in *C. elegans* is largely mediated through distinct receptor-type guanylyl cyclases (rGC proteins, encoded by *gcy* genes), which confer salt specificity via their extracellular domains (*30*) . Our previous genome survey of *Ppa* homologs of *gcy* genes has revealed patterns that made us question whether *Ppa gcy* genes are convincing candidates for lateralized chemotactic responses. Specifically, we noted that ASER-expressed *C. elegans gcy* genes and ASEL-expressed *C. elegans gcy* genes have only expanded in the *Caenorhabditis* genus (*11*). One outlier to this pattern is the *Cel-gcy-22* gene, which is expressed in ASER, but has not expanded in *C. elegans* (*11*, *42*). However, this gene has duplicated several times in *P. pacificus,* resulting in 5 putative *Ppa-gcy-22* paralogs (*11*). We fused the promoter of one of these paralogs, *Ppa-gcy-22.3,* to *gfp* and found that transgenic animals express GFP exclusively in ASER (Fig. 6A), identical to the *C. elegans gcy-22* ortholog (*42*). We confirmed its expression in ASER by analyzing animals that carry both the *Ppa-gcy-22p::gfp* reporter and the *Ppa-che-1p::rfp* reporter, showing a unilateral overlap of these reporters in ASER (Fig. 6B).

To assess whether *Ppa-gcy-22.3* is a potential effector of *Ppa-che-1* function, we crossed the *gcy-22.3* reporter into *che-1(ot5012)* mutants. We found expression of *gcy-22.3* was eliminated (Fig. 6C), leading us to conclude that *gcy-22.3* is a potential effector of *che-1* function, identical to its homolog in *C. elegans*.

To determine whether and which of the observed salt responses is mediated by the ASER-expressing *gcy-22.3*, we generated a putative *gcy-22.3 null* mutant through CRISPR/Cas9 genome editing (2 bp complex deletion that introduces a frameshift)(Fig. 7A) and examined its response to the higher salt concentration. The ‘OFF’ response to 250 mM NH_4Cl was notably abolished in the ASER neuron in the loss-of-function *gcy-22.3* mutant, while the ‘ON’ response in the ASEL remained intact (Fig. 7B-C). However, the responses to 250 mM NaCl were not significantly reduced in the either the ASEL or ASER neuron in the *gcy-22.3* mutant (Fig. 7D-E). Furthermore, the *gcy-22.3* mutation also reduced the ‘ON’ portion of the AFD biphasic response following presentation of 250 mM NH_4Cl and NaCl (Fig. 7F-G). We also examined the behavioral responses toward individual salt ions in *gcy-22.3* mutants, including a second loss-of-function allele *csu182*. Overall, we found no significant differences between wildtype and mutants in responses

towards individual ions, and only the attraction to NH_4Cl was slightly enhanced in both alleles (Fig. 8), which was unexpected given the lack of calcium response observed in *gcy-22.3*(*csu181)* towards NH_4Cl. Our findings show that while proper ASE function is critical for salt attraction, defects in individual *gcy* genes do not lead to a major impact on the worms' ability to track toward attractive salts.

Discussion

Our study has revealed several insights into the substrates of evolutionary changes between two distantly related nematode species, *P. pacificus* and *C. elegans*. We used intracellular calcium levels as our readout for neuronal activity with a genetically encoded calcium sensor in two pairs of *che-1*-expressing amphid sensory neurons– the first calcium imaging study in *P. pacificus*. We show that three neuron types (ASE left, ASE right and AFD neurons) each have distinct calcium responses to specific ion concentrations, revealing diversity at the single neuron level. We have identified the first laterally asymmetric marker in *P. pacificus*, *gcy-22.3p::GFP,* with its expression limited to ASER homolog (AM7). Our unexpected discovery that neuronal asymmetry is present in the ASE homologs between two distantly related nematode species, despite the lack of a *lsy-6* homolog, suggests that functional lateralization in *P. pacificus* may be mediated by a different genetic pathway compared to *C. elegans*.

***P. pacificus* and *C. elegans* have diverged taste palates**

We have shown that while *C. elegans* is attracted to acetate salts, *P. pacificus* avoids these acetates. Previous studies have shown that ammonium acetate (NH_4Ac) is sensed both as a water-soluble compound as well as a volatile odorant and is mediated by different signaling pathways (*36*). Like *C. elegans*, it is therefore likely that ammonium and acetate ions involve a different set of neurons in *P. pacificus* (*i.e.* non-*che-1* expressing neurons), based on the finding that histamine-treated *che-1p::HisCl1* animals did not significantly attenuate their repulsive response to NaAc. We find that sodium chloride is a common attractant for both *P. pacificus* and *C. elegans*, although the magnitude of response is lower than previously published results (*29*). This result is likely due to differences in generating the salt gradients. Nevertheless, we find that *P. pacificus* neurons have a distinct response to this salt when compared to those observed in *C. elegans* neurons. The *P. pacificus* ASEL neuron responds to a decrease in NaCl concentration (likely sodium), as evidenced by the 'OFF-2' response profile, whereas the *C. elegans* ASEL neuron responds to an increase in sodium concentration. However, in both nematodes, the ASER neuron responds to a decrease in chloride concentration. Additionally, the *P. pacificus* ASER neuron exhibits a unique ON-OFF response to

ammonium iodide, whereas in *C. elegans*, no ON-OFF type of response is seen in the ASE neurons– the *C. elegans* ASER neuron responds only to a decrease in iodide concentration. Based on our calcium imaging and chemotaxis results on the *gcy-22.3* mutants, attraction to ammonium ions (NH_4^+) is likely mediated in part by the ASER neuron in *P. pacificus*. *Pristionchus* species are entomophilic and most frequently found to be associated with beetles in a necromenic manner and thus insect cadavers could be sources of ammonium in the soil (*6*, *43–45*) . Additionally, ammonium salts could represent a biological signature of other nematodes that the predatory morph of *P. pacificus* could interpret as prey. In *P. pacificus,* nutritional state has a measurable role in the mouth-form polyphenism decision between predatory and non-predatory morphs (*46*). Collectively, our findings highlight the divergence of the *P. pacificus* salt-sensory neurons compared to those observed in *C. elegans*.

***P. pacificus* ASE neurons have narrower sensitivity range**

The sensitivity range of the *P. pacificus* ASER responses is significantly less compared to the ASEL responses, as well as to *C. elegans* ASER responses. Whereas the *C. elegans* ASER has a 40-fold sensitivity range in the 'OFF' response to the removal of various concentrations of NaCl (1-40 mM)(*29*, *47–49*), the *P. pacificus* ASER showed the 'OFF' response only to 250 mM NH_4Cl but not to a 10-fold reduction in concentration of NH_4Cl (25 mM). For the ASEL in contrast, the response to 25 mM was just as strong as to 250 mM NH_4Cl (10-fold) and comparable to the 8-fold concentration range observed for *C. elegans* ASEL towards NaCl. Alternatively, the magnitude of these sensitivity differences may be also partially due to differences among calcium indicators (*i.e.* GCaMP and Cameleon), but multiple *P. pacificus che-1p::GCaMP* strains did not exhibit sufficient basal fluorescence to allow for image tracking and direct comparison. The narrower sensitivity range in *P. pacificus* chemosensation was also observed for attraction to volatile odors (*2*), which span only 10-fold, versus up to 10,000-fold in attractive odors for *C. elegans* (*21*).

***P. pacificus* taste neurons exhibit a unique biphasic response**

Although the left-ON and right-OFF responses are conserved in the ASE neurons in both species, the biphasic response of ASER to 250 mM NH_4I has not been observed in either of the ASE neurons towards salts. In *C. elegans*, hyperosmotic stimulus such as 1M glycerol, or high concentrations or long duration of $CuSO_4$ exposure both result in biphasic responses by the ASH neurons that sense noxious chemicals (*41*, *50*). Olfactory neurons that mediate avoidance behavior such as the AWB neurons can also exhibit a biphasic response to the presence and removal of a high concentration isoamyl alcohol that normally elicits avoidance behavior (*51*). The neuron-specific response can also be dependent on the concentration of the chemical compound, since the ASER to 25 mM NH_4I was a weak 'OFF' rather than a biphasic one. In contrast to the salt-dependent response types by *P. pacificus* ASE neurons, the *P. pacificus* AFD neurons also show exclusively biphasic responses with various amplitudes. Further characterization will help determine if biphasic responses can also be found in other sensory neuron types in *P. pacificus*, specifically those neurons mediating avoidance behavior.

AFD are potentially polymodal neurons

Broadly speaking, *C. elegans* chemosensory neurons have been classically characterized as specialized neurons for dedicated modalities such as water-soluble chemicals (ASE), volatile odorants (AWA, AWB, AWC), noxious chemicals (ASH), pheromones (ADL, ADF, ASK), as well as light (ASJ) and temperature (AFD)(*1*, *37*, *52–55*). Advances in multi-neuron calcium recordings have since shown that a given odor within a certain concentration range is detected by different ensembles of the 12 amphid neuron classes, including the AFD neurons (*56–58*). Unexpectedly, we found that the *P. pacificus* AFD neurons exhibit a distinctive biphasic response to all three salts tested (NH_4Cl, NaCl, and NH_4I), which differ from the *C. elegans* AFD calcium responses (*58*, *59*). Moreover, the loss of the receptor *gcy-22.3* reduced the AFD 'ON' response to NH_4Cl and NaCl, indicating ASER contributes to the AFD response. The strong positive AFD response to 25 mM NaCl that is absent in both ASE neurons further supports the likelihood that AFD receives inputs from other amphid neurons. The integration of thermosensation and chemosensation is important for memory-regulated behavior. In *C. elegans,* maximum chemotaxis indices toward NH_4Cl occurs when there is concordance

between cultivation temperature and assay temperature (*60*). The *C. elegans* AFD neurons are also important for gustatory aversive learning in NaCl avoidance (*49*). Given the influence of environmental temperature on the *P. pacificus* mouth-form plasticity and the wide range of micro-climates that wild strains of *P. pacificus* have been isolated from (*61–63*), temperature and taste preferences could be regulated at multiple genetic levels during crucial developmental decisions.

Changes in the gene regulatory architecture of sensory neuron specification

We found that the key regulator of *Cel* ASE identity, *che-1,* is also expressed in *Ppa* ASE and may play a similar role as a terminal selector in this neuron type, based on its effect on ASE-mediated behavior and regulation of the *Ppa-gcy-22.3* gene. However, the stronger behavioral effect of silencing of *che-1* expressing neurons compared to a *che-1* mutant background could either indicate that *che-1* does not have as broad a role in controlling ASE differentiation in *P. pacificus* versus *C. elegans*. It is possible that a developmental loss of ASE differentiation may result in compensatory changes in the chemosensory system during early development, as was observed in the *C. elegans* mating pheromone response by males (*64*). It is also worthwhile to note that *Cel-gcy-22* stands out for being located on a separate chromosome (Chr. V) compared to the other ASER-type *gcy* genes (*gcy-1, gcy-4, gcy-5* on Chr. II) as well as the *Cel-gcy-22* mutant having defects in chemoattraction towards a wide range of salt ions (*30*, *42*). Given that the 5 *P. pacificus gcy-22*-like paralogs are located on 3 separate chromosomes (Chr. I, IV, X), it is likely that they emerged from independent and repeated gene duplication events after the separation of *Caenorhabditis* and *Pristionchus* lineages. Although the promoter fusion reporters of other *gcy* genes have been uninformative due to lack of expression (*Ppa-gcy-22.1*, *Ppa-gcy-7.1, Ppa-gcy-7.2*, *Ppa-gcy-5*), it is likely that ASEL-specific *gcy* genes as well as additional ASER-specific *gcy-22*-like genes exist. Finding other genes with left-right specific expression could help to identify genetic determinants affecting lateral asymmetry.

Unexpectedly, we found that unlike in *C. elegans,* the *Ppa-che-1* gene is also expressed in the AFD neurons. Since we cannot record neural activity in AFD in a *che-1* mutant (the *che-1p::RCaMP* driver fails to be expressed sufficiently in *che-1* mutants due

to autoregulation), and do not yet have molecular markers for *Ppa* AFD neurons, we cannot assess whether *che-1* affects AFD neuron differentiation.

Perhaps the most striking difference in the gene regulatory architecture of ASE neuron specification is the apparent lack of the key regulator of ASE asymmetry in *P. pacificus*, the miRNA *lsy-6.* In *C. elegans,* the expression of *lsy-6* exclusively in ASEL is prepatterned via an early embryonic Notch signal (*33*) and serves to downregulate the homeodomain transcription factor *cog-1* in the ASEL neuron (*65*). Through a network of downstream regulatory events, asymmetry of rGCs eventually becomes established (*31*). *cog-1* and several asymmetrically expressed downstream effectors of *cog-1*, such as the *die-1, lim-6* and *fozi-1* transcription factors are conserved in *P. pacificus,* but whether the function of these factors in controlling *P. pacificus* ASE laterality is conserved remains to be determined. In this context it is intriguing to note that another prominent gene regulatory pathway that is controlled by miRNAs in *C. elegans*, the heterochronic pathway (*let-7s, lin-4*), appears to have diverged in *P. pacificus* as well, despite the conservation of the overall physiological readouts of this pathway (temporal patterning of cell lineage divisions)(*66*). It is tempting to speculate that miRNA-meditated regulatory process is particularly labile.

In conclusion, our work illustrates how comparative behavioral and genetic analyses in nematodes is a powerful strategy to uncover substrates of evolutionary change in simple nervous systems.

Materials and Methods:

Nematode Strains

P. pacificus and other nematode strains were maintained at ~20°C on NGM plates seeded with *E. coli* OP50 for food as described previously (*67*); these are derived from standard *C. elegans* culture methods (*68*). *P. pacificus* and other nematode strains used are listed in Table S1.

Chemotaxis assays

The assay for assessing response to salt gradients was adapted from *C. elegans* and *P. pacificus* chemotaxis assays (*2*, *21*, *42*). Overnight salt gradients were established on 10 cm chemotaxis plates containing 20 ml agar (5 mM KPO4, 1 M $CaCl_2$, 3% Bacto-agar, 1 mM $MgSO_4$) by adding 10 µl of 2.5 M salt solutions for 16 hours. Alternatively, agar containing 25 mM (NH_4Cl, NH_4I) or 50 mM (NaCl) were used to test for responses to individual salt ions. Following the establishment of the overnight point gradient, another 4 µl of the same salt solution or water control was added to reinforce the gradient 4 hours before the assay. Just prior to the assay, 1 µl of 1 M sodium azide was added to both the attractive salt (A) and the control (C) spots. *P. pacificus* J4 to adult hermaphrodites from near-saturated cultures were washed 3x with distilled water and collected by centrifuging at 2000 rpm for 2 minutes. Approximately 200 worms were loaded onto the edge of each assay plate between the gradient sources, and at least 10 combined worms have to reach the scoring arenas to be considered. At least 10 assays constituted each experimental trial, and multiple trials were conducted and averaged for each condition. The Chemotaxis Index (CI) for each end-point assay plate is defined as (A - C)/(A + C). To conduct conditional knockdowns of neurons, 5 M histamine dihydrochloride (Sigma Aldrich H7250) stock solution in sterilized deionized water (Arrowhead CA) was filter-sterilized and top plated onto the agar plates to a final histamine concentration of 25 mM histamine approximately 10 minutes before loading the worms to commence the assay. Most assays lasted 3-4 hours at room temperature to allow *P. pacificus* sufficient time to reach the scoring arenas, with ~40% of the animals participating. When using the *csuEx83[Ppa-che-1p::optHisCl1]* strain, only animals expressing *Ppa-egl-20p::RFP* tail marker from the extrachromosomal array were scored. Because of *P. pacificus'* strong aversion to acetate,

we could not easily assess the individual contributions of salt ions in a saturated background of ammonium acetate as conventionally practiced in *C. elegans* studies (*30*).

Ppa-che-1p::HisCl1 **strain**

To make the *Ppa-che-1p::optHisCl1*, the *P. pacificus* codon-optimized histamine-gated chloride channel sequence used in *C. elegans* (*HisCl1)*(*69*, *70*) was designed using (https://hallemlab.shinyapps.io/Wild_Worm_Codon_Adapter/)(*71*) and custom synthesized (Twist Bioscience), and subsequently inserted behind the *che-1* promoter (3.1 kb containing the first exon and intron)(*11*) to create the pHC30 plasmid construct. This *Ppa-che-1p::optHisCl1* plasmid (2 ng/µl) along with PS312 genomic DNA (80 ng/µl) and *Ppa-egl-20p::RFP* co-injection marker (2 ng/µl) were individually digested with HindIII and assembled as the injection mix to create *csuEx83*.

Ppa-che-1p::RCaMP **reporter strain**

To make the *Ppa-che-1pei::optRCaMP*, we generated a transgenic worm strain expressing the codon-optimized genetically-encoded calcium indicator (GECI), jRCaMP1a, in the neurons of interest (*72*, *73*). jRCaMP1a is an improved red GECI based on mRuby with comparable sensitivity to GCaMP6 (*74*). The codon-optimized RCaMP sequence was custom synthesized (Twist Bioscience), and then subcloned using the plasmid pJET1.2/blunt (Thermo Fisher Scientific) to create the pMM2 plasmid construct. Using Gibson Assembly (E2611, New England Biolab), the codon-optimized *RCaMP* sequence was introduced downstream of the *Ppa-che-1* promoter sequence with the first exon and intron sequences to create the pMM5 plasmid construct. Separately, we also generated a *Ppa-che-1pei::optGFP* transcriptional reporter with codon-optimized *GFP* (pMM3) to enable the localization of the *che-1*-expressing neurons during video acquisition (*75*). The *Ppa-che-1pei::optRCaMP* (2 ng/µl) and *Ppa-che-1pei::optGFP* constructs (1 ng/µl), along with PS312 genomic DNA (80 ng/µl) and *Ppa-egl-20p::RFP* (1.5 ng/µl) were individually digested with HindIII and assembled as the injection mix to create *csuEx93*. Despite multiple attempts, we were unable to generate an equivalent *che-1pei::GCaMP* transgenic line with sufficient basal level of GCaMP expression for a comparison to the RCaMP calcium dynamics.

Promoter fusion reporter strains

The *Ppa-gcy-22.3p::GFP* construct contains 899 bp of the upstream promoter of the PPA04554 transcript is fused to the codon-optimized GFP (pVL2). A shorter *gcy-22.3* transcript with different first two exons is also predicted, which is more similar in length to other rGC genes in *P. pacificus* (Contig12-snapTAU.506). The *Ppa-ttx-1pei::RFP* construct contains 1935 bp of the upstream promoter along with the first exon and intron sequences of *Ppa-ttx-1* (PPA26714) fused to the codon-optimized RFP, excluding the first 2 codons (pDC14). pVL2 (2 ng/µl) or pDC14 (2 ng/µl), along with PS312 genomic DNA (80 ng/µl) were individually digested with HindIII to create the injection mixes to generate the independent reporter strains, *csuEx90[Ppa-gcy-22.3p::GFP],* as well as *Ppa-ttx-1pei::RFP(csuEx94)* and *Ppa-ttx-1pei::RFP(csuEx96)*. *csuEx96* showed less gland cell expression (which can occlude neuronal expression) and stronger AFD expression than *csuEx94*.

CRISPR mutagenesis generated mutants

CRISPR/Cas9 mutagenesis was used to generate mutations (*75*, *76*). crRNA and primer sequences, and induced mutations, are included in Table S3 and Fig. S8.

***che-1* alleles (PPA01143)**: Target crRNA, tracrRNA, and Cas9 nuclease were purchased from IDT Technologies (San Diego, CA). crRNA and tracrRNA were hydrated to 100 µM with IDT Duplex Buffer, and equal volumes of each (0.61 µl) were combined and incubated at 95°C for 5 minutes, then 25°C for 5 minutes. Cas9 protein (0.5 µl of 10 µg/µl) was added, then the mix was incubated at 37°C for 10 minutes. *Ppa-egl-20p::RFP* was used as a co-injection marker. To reach a final total volume of 40 µl, the Cas9-crRNA-tracrRNA complex was combined with pZH009 (*Ppa-egl-20p::RFP*) DNA to reach 50 ng/µl final concentration using nuclease-free water. F_1 progeny were screened for the presence of *Ppa-egl-20p::RFP* expression in the tail and candidate F_1's were sequenced to identify heterozygotes (*76*). *ot5012* has a 4 bp insertion while *ot5013* has an 8 bp complex insertion/deletion, and both mutations cause frameshift mutations and premature stop codons. Each allele was outcrossed two times to wildtype before characterization.

***gcy-22.3* alleles (PPA04454):** Target crRNA, tracrRNA, and Cas9 nuclease were purchased from IDT Technologies (San Diego, CA). crRNA (RHL1400) and tracrRNA

were hydrated to 100 µM with IDT Duplex Buffer, and equal volumes of each (0.61 µl) were combined and incubated at 95°C for 5 minutes, then 25°C for 5 minutes. Cas9 protein (0.5 µl of 10 µg/ µl) was added, then the mix was incubated at 37°C for 10 minutes. *Ppa-egl-20p::RFP* was used as a co-injection marker. To reach a final total volume of 40 µl, the Cas9-crRNA-tracrRNA complex was combined with pZH009 (*Ppa-egl-20p::RFP*) DNA to reach 50 ng/µl final concentration using nuclease-free water. F_1 progeny were screened for the presence of *Ppa-egl-20p::RFP* expression in the tail and candidate F_1's were sequenced to identify heterozygotes (*76*). *csu181* has a 2 bp complex deletion, while *csu182* has a 22 bp complex deletion, both mutations cause frameshifts and premature stop codons. Each allele was outcrossed two times to wildtype before characterization.

ALFA C-terminal tagging and immunostaining: For induction of site-specific insertions via CRISPR/Cas-9 mediated mutagenesis, target crRNA, tracrRNA, and Cas9 nuclease were treated as described above. Single-stranded DNA repair template containing the ALFA nanobody tag (RHL1551 for CHE-1 and RHL1519 for TTX-1) with 35 bp of homology arms on the 5' and 3' sides were purchased from IDT. To minimize sequence identity, the two copies of the ALFA sequence contain silent mutations. The crRNA (RHL1396 for *che-1* and RHL1514 for *ttx-1*) and tracrRNA were hydrated to 100 µM with IDT Duplex Buffer, and equal volumes of each (0.61 µl) were combined and incubated at 95°C for 5 minutes, then 25°C for 5 minutes. The ALFA tag was C-terminally inserted to the longest *ttx-1* splice form in the last 18th exon (ppa_stranded_DN30925_c0_g1_i5)(Trinity 2016 transcripts can be found on www.pristionchus.org). F_1 animals expressing the co-injection marker *egl-20::optRFP* were lysed and checked by PCR for insertions.

Non-starved healthy cultures of ALFA-tagged CHE-1 (*csu226*[*Ppa-che-1*::2xALFA]) or ALFA-tagged TTX-1 (*RLH280*[*Ppa-ttx-1*::2xALFA]) (from six 6 cm plate cultures) were washed with M9 and filtered (Sartorius 84g/m2, Grade 392) and processed as previously described (*39*). In brief, mixed stage worms were fixed overnight at 4°C on a nutator with 500 µl fixation buffer (4% paraformaldehyde in PBS). The worms were then incubated overnight at 37°C with 500 µl 4% β-mercaptoethanol dissolved in 1% Triton-X100 in 0.1M Tris pH 7.4, and digested in 200 µl of collagenase buffer with 200 units of collagenase type IV (Gibco, Thermo Fisher Scientific, Waltham, MA, USA) at 37°C for ~3.5 hours. The

partially digested worms were subsequently washed three times with 500 µl PBST. After collagenase treatment the centrifugation between the washes was done at low speed, 1000 RCF. After washes, the worms were stained in 50 µl 1% BSA in PBST with the primary antibody (1:100 FluoTag-X2 anti-ALFA-AZdye568, N1502, NanoTag Biotechnologies, Göttigen, Germany), overnight at 4°C in a nutator. Following the washes, worms were resuspended in 50 µl VectaShield mounting medium (H-1000, Vector Laboratories, USA) containing DAPI (Molecular Probes, Thermo Fisher Scientific) and gently mounted on freshly prepared 3% Noble agar pads. Images were acquired on a Leica DM6000 microscope.

Calcium Imaging

To conduct calcium imaging, worms were trapped and imaged within a microfluidic PDMS chip while delivering stimuli directly to the nose of an immobilized worm, as previously described (*50*, *77*). The microfluidic chip was connected to a programmable valve controller (ValveBank) that enables the user to toggle between “stimulant ON” and “stimulant OFF” states. Specifically, the ValveBank allows controlled switching of flow from the two outer buffer channels in the chip such that either the control solution (stimulant OFF) or the stimulant solution (stimulant ON) flows over the worm nose (Fig. S9). Buffer solution (for the outer two channels) consisted of M9 buffer with 0.1% Tween-20 and 1 µg/ml fluorescein (*78*, *79*). The worm loading solution consisted of M9 buffer with 0.1% Tween-20 and 1.5 mM tetramisole hydrochloride to immobilize the animal. Water-soluble stimulant solutions consisted of the following water-soluble compounds dissolved in nanopure/milli-Q water: ammonium chloride (NH_4Cl), ammonium iodide (NH_4I), and sodium chloride (NaCl) at concentrations of 250 mM and 25 mM. 750 mM NaCl elicited very inconsistent responses. The water-soluble stimulant solution was made by diluting the water-soluble compound in nanopure/milli-Q water with 0.1% Tween-20. The control solution consisted of 0.1% Tween-20 nanopure/milli-Q water. Worms were exposed to the control solution, stimulant solution, and then control solution using a 60-second program: 10 seconds stimulant OFF, 20 seconds stimulant ON, and 30 seconds stimulant OFF. As a negative control, animals were exposed only to the control solution, without switching channels, for the duration of the recording. For each animal,

the orientation of the nose and vulva were recorded and used as a guide to determine the ventral and dorsal sides of the worm, and subsequently, the left and right sides of the worm. Accounting for the plane of focus of the neuron pairs as viewed through the microscope, it was then determined whether the imaged neuron was the worm's left or right neuron of each pair. Images were captured using a Zeiss Axio Observer Z1 inverted fluorescence microscope and a pco.panda 4.2 sCMOS camera. Changes in fluorescence intensity were measured in the neurons of interest while the worm was exposed to green light. Images were processed using MetaMorph software version 7.10.5.476. Images were captured at 500 ms exposure time at 2 fps because the baseline fluorescence in *Ppa-che-1p::optRCaMP* worms was too dim to capture viable data using the standard 100 ms exposure time. Baseline F_0 was measured as the average background-subtracted fluorescence from the first 9 seconds of each recording and change in fluorescence intensity was calculated as $dF/F = (F - F_0) / F_0$, as described (*79*). Data were analyzed and plotted using custom scripts generated in MATLAB versions R2021a–R2024a. This code is available at https://github.com/honglabcsun/Calcium-Imaging.

For bar plot comparisons between wildtype and *gcy-22.3* mutants, we calculated minimum pre-stimulus and maximum post-stimulus % dF/F values using custom scripts generated in MATLAB. Min-Max data were exported as text files, manually converted and organized into an XLSX file (Microsoft Excel Office16) and imported into Prism GraphPad software (version 10) for data visualization and statistical analysis.

Nomenclature: Throughout the results section, *P. pacificus* genes will be referred to without the *Ppa-* prefix; if necessary for comparison to another species such as *C. elegans (Cel-)* the *Ppa-* prefix will then be used.

Table 1. Comparison of ASEL/R responses between *P. pacificus* and *C. elegans*.

	P. pacificus		*C. elegans*	
	ASEL	**ASER**	**ASEL**	**ASER**
NH_4Cl (1 – 80mM)	ON	x	x[29,30]	OFF[29,30]
NH_4Cl (81 – 250mM)	ON	OFF	?	?
NaCl (1 – 80mM)	x	OFF	ON[29,43-45]	OFF[29,43-45]
NaCl (81 – 250mM)	OFF-2	OFF	ON[44]	OFF[44]
NH_4I (1 – 80mM)	ON	OFF	X[30]	OFF[30]
NH_4I (81 – 250mM)	ON	ON-OFF	?	?

"x" minimal to no response
"?" represents unknown

Figures:

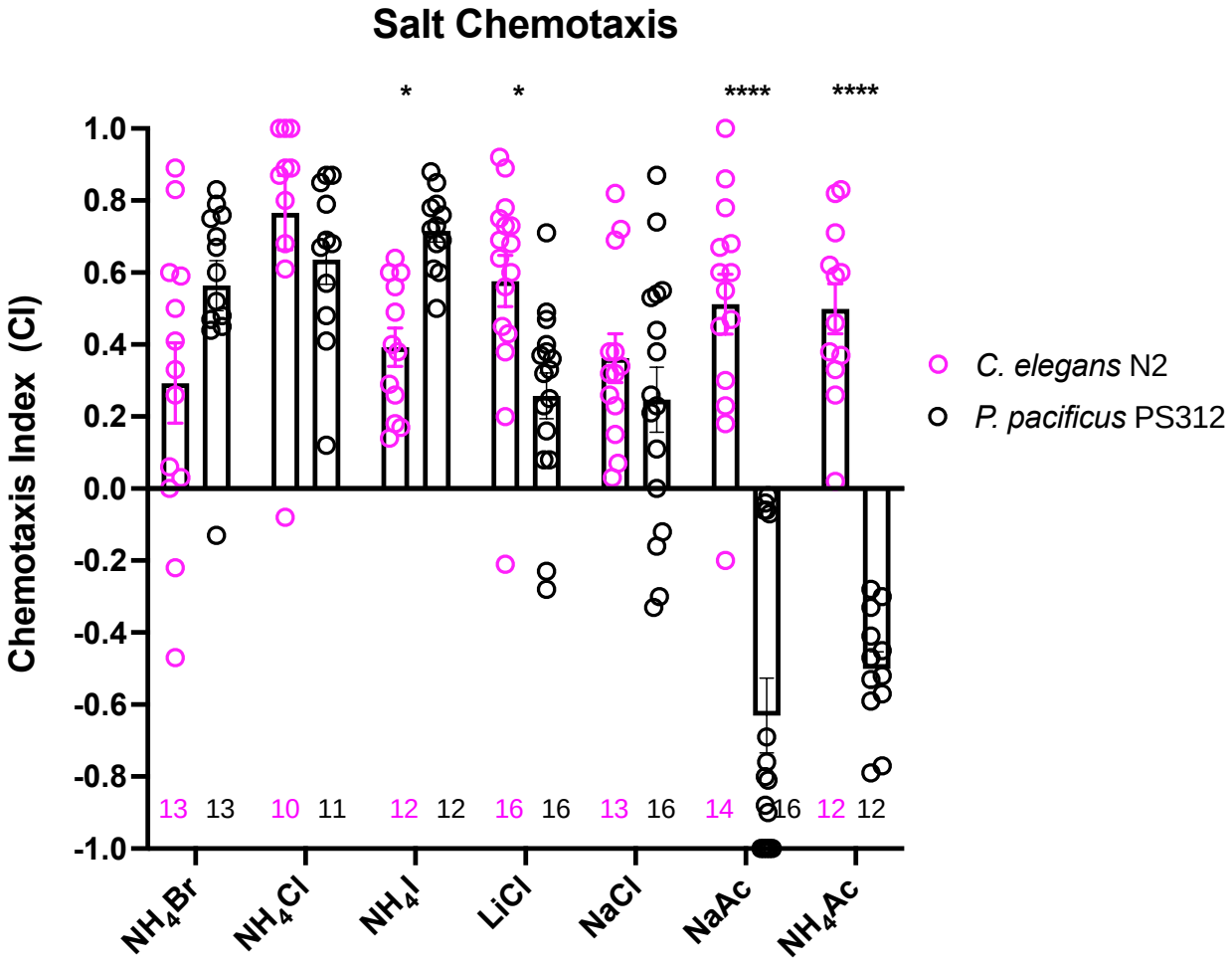

Figure 1. A comparison of chemotaxis responses to water-soluble ions between *P. pacificus* and *C. elegans*. J4 to Adult hermaphrodites from the two species responded to NH_4I, LiCl, and acetates significantly differently. Using two-way ANOVA, significant difference found between wildtype *P. pacificus* and *C. elegans* for the same salt is indicated above each pair (*$p<0.05$, ****$p<0.0001$), while the differences within *P. pacificus* is as follows: all salts showed difference when compared to NaAc and to NH_4Ac(****$p<0.0001$), but not between NH_4Ac and NaAc. Both LiCl and NaCl attraction are significantly lower than NH_4Cl (*$p<0.05$) and NH_4I (***$p<0.001$). Error bars denote standard error of the mean and the sample sizes are indicated on the bottom.

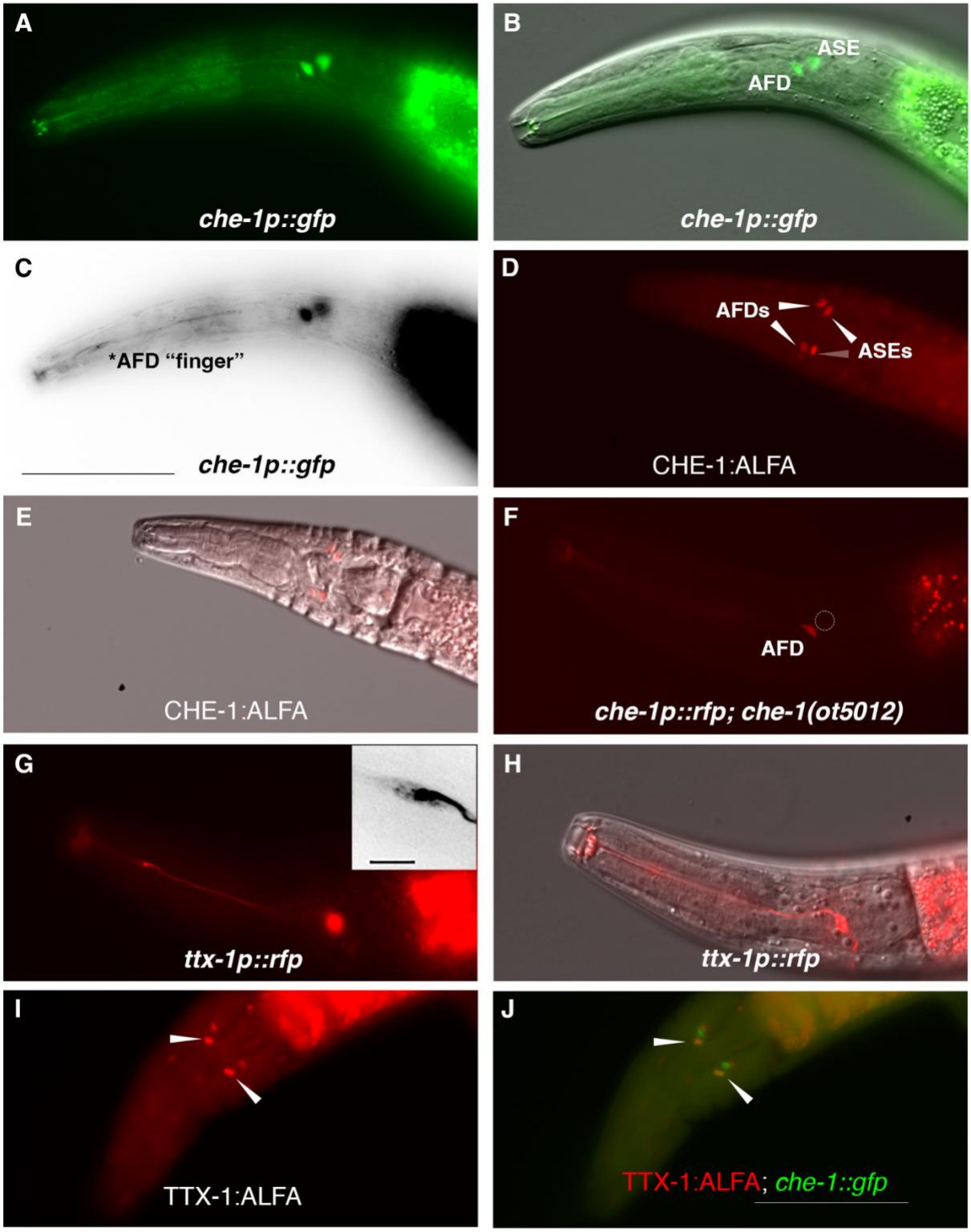
A
che-1p::gfp
B
ASE
AFD
che-1p::gfp
C
*AFD "finger"
che-1p::gfp
D
AFDs
ASEs
CHE-1:ALFA
E
CHE-1:ALFA
F
AFD
che-1p::rfp; che-1(ot5012)
G
ttx-1p::rfp
H
ttx-1p::rfp
I
TTX-1:ALFA
J
TTX-1:ALFA; che-1::gfp

597

Figure 2. *P. pacificus che-1* expression in ASE and AFD amphid neurons. (A-B) The *che-1::GFP* marker in the *che-1::RCaMP* reporter strain is expressed in the ASE and AFD amphid neurons. (C) *che-1::GFP* expression is detectable in the morphologically distinct AFD neurons with 'finger'-like dendritic endings. (D-E) Immunostaining of *CHE-1::ALFA* shows two pairs of amphid neuron cell bodies corresponding to the ASE and AFD neurons; dorsal-ventral view (n=114). (F) The loss of *che-1* results in loss *che-1::RFP* expression in the ASE (circle) while retaining reduced AFD expression. (G) *ttx-1p::RFP* expression in the AFD neurons with 'finger'-like dendritic endings. Inset shows expanded inverted black-white image of the AFD dendritic ending. (H) AFD expression of the same *ttx-1::RFP* animal shown in (G) in a different plane with cell body in focus. (I-J) Immunostaining of *TTX-1::ALFA* (red) shows one pair of amphid neuron cell bodies co-localizing with the anterior pair of *che-1::GFP*-expressing AFD neurons (yellow); dorsal-ventral view (n=13). Anterior is left and the scale bar in (C) represents 50 µm for all panels except for the G inset, which is 5 µm.

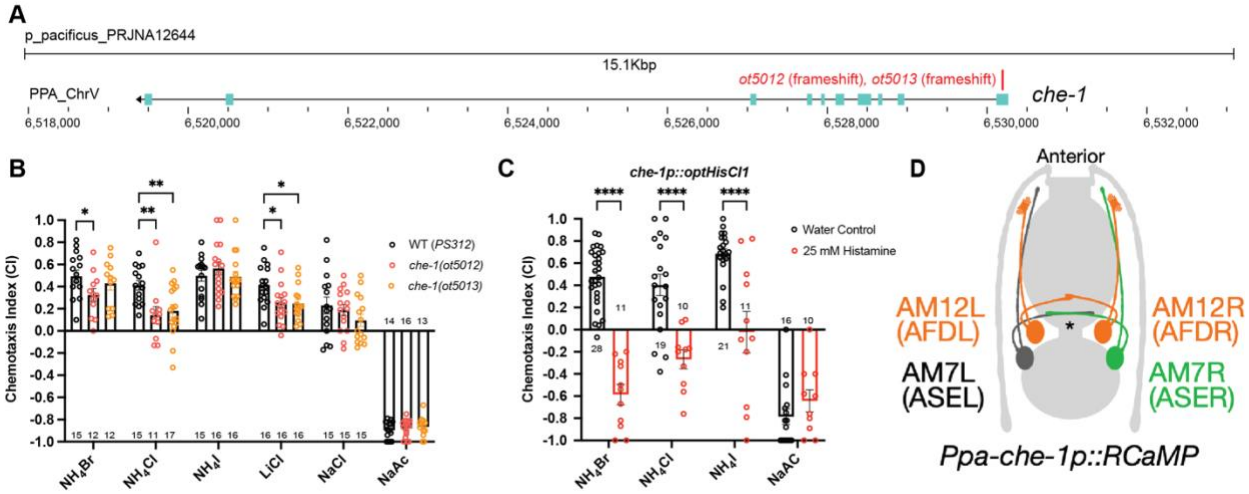

Figure 3. *che-1* expressing amphid neurons are required for sensing water-soluble ions in *P. pacificus*. (A) The *che-1* locus with CRISPR/Cas9- induced mutations in Exon 1. (B) The *che-1* mutants show defects in attraction towards NH_4Br, NH_4Cl, and LiCl. Sample sizes are indicated below for attractants and above for repellent. (C) The *che-1p::HisCl1* animals lose attraction towards NH_4Br, NH_4Cl, and NH_4I in a histamine dependent manner. Sample sizes are indicated at the base of each bar. (D) A schematic map of the *P. pacificus* AM7(ASE) and AM12(AFD) amphid neurons that express the *che-1p::RCaMP* used in calcium imaging. The ASE axons are the only amphid axons in *P. pacificus* to cross each other over the dorsal lateral midline contralaterally. **P<0.01, *P<0.05 Two-way ANOVA with Dunnett's post-hoc comparison showing alleles with significant difference to wildtype *P. pacificus* (PS312). ****P<0.0001 Two-way ANOVA showing significant difference between water control and histamine treatment.

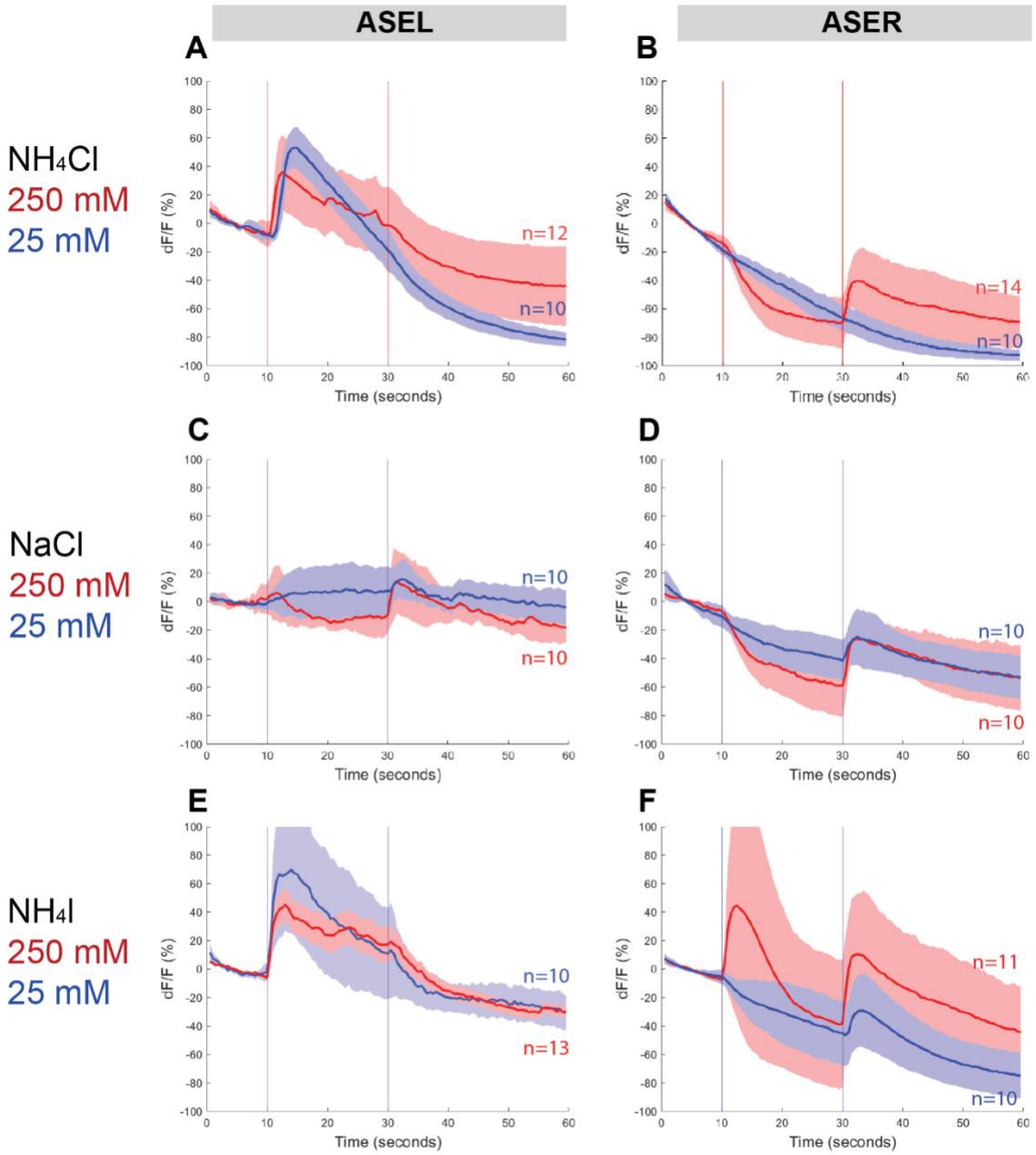
ASEL
ASER
A
B
C
D
E
F
NH4Cl
250 mM
25 mM
NaCl
250 mM
25 mM
NH4I
250 mM
25 mM
dF/F (%)
Time (seconds)
n=12
n=10
n=14
n=10
n=10
n=10
n=10
n=10
n=10
n=13
n=11
n=10

626

Figure 4. ASEL and ASER responses to different concentrations of NH_4Cl, NaCl, and NH_4I. Average percent change in RCaMP fluorescence (dF/F) over time (seconds) of tracked ASE (left and right) sensory neurons in *P. pacificus*. Salts were presented at 10s ("ON", left vertical line) for a duration of 20s, and then removed ("OFF", right vertical line) for the remaining 30s; the total recording time was 60s. (A-B) ASEL and ASER neuron responses to high (250 mM, red) compared to low (25 mM, blue) concentrations of NH_4Cl. (C-D) ASEL and ASER neuron responses to NaCl. (E-F) ASEL and ASER neuron responses to NH_4I. Shaded ribbons represent 95% confidence intervals. Shaded ribbons in (E-F) have been cropped to maintain consistent y-axes across the plots, allowing for easier comparison. Sample sizes are indicated (n).

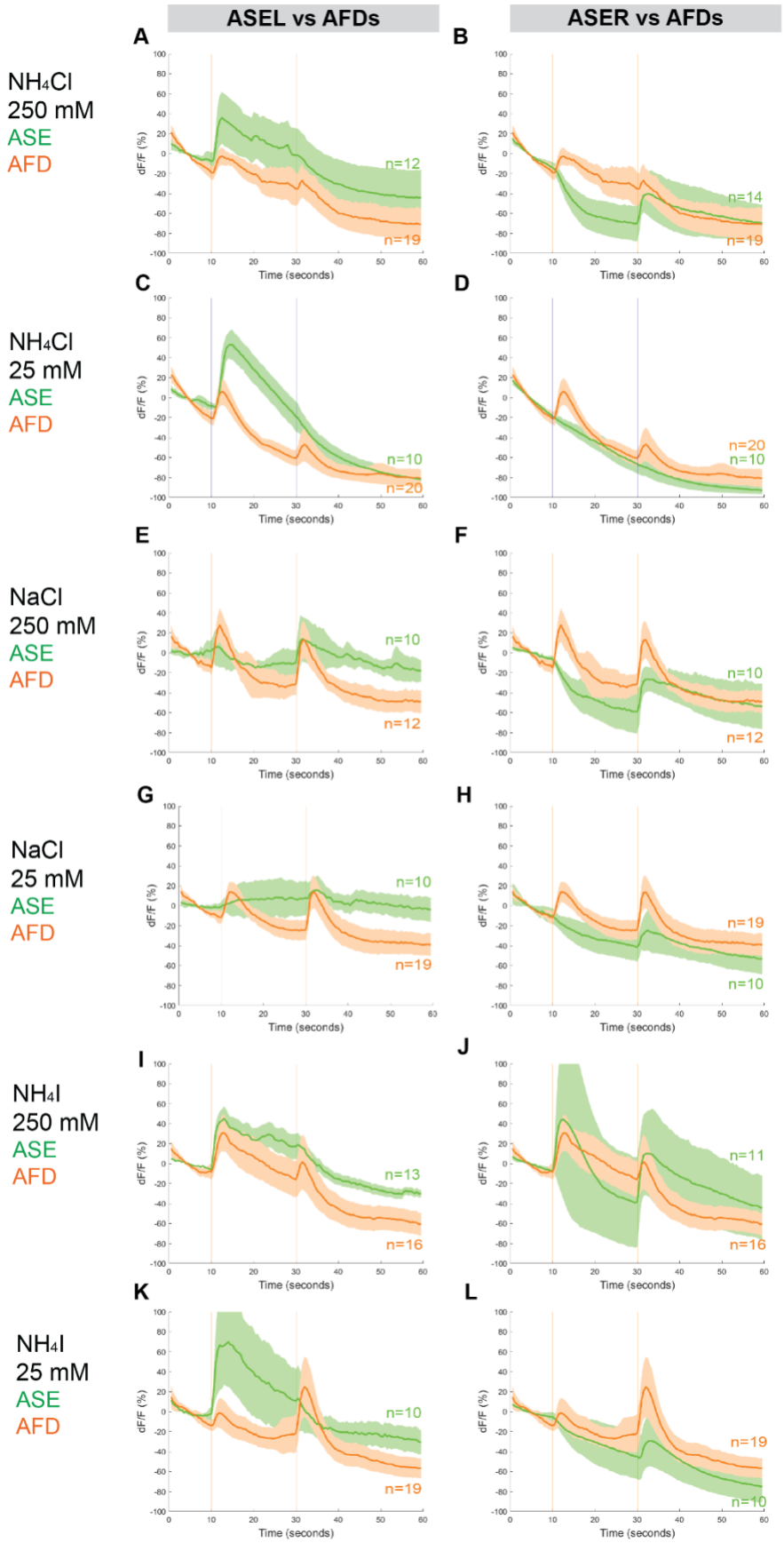
ASEL vs AFDs
ASER vs AFDs
A
B
C
D
E
F
G
H
I
J
K
L
NH4Cl
250 mM
ASE
AFD
NH4Cl
25 mM
ASE
AFD
NaCl
250 mM
ASE
AFD
NaCl
25 mM
ASE
AFD
NH4I
250 mM
ASE
AFD
NH4I
25 mM
ASE
AFD
dF/F (%)
Time (seconds)
n=12
n=19
n=14
n=19
n=10
n=20
n=20
n=10
n=10
n=12
n=10
n=12
n=10
n=19
n=19
n=10
n=13
n=16
n=11
n=16
n=10
n=19
n=19
n=10

637

Figure 5. Combined AFD responses in comparison to ASE left or right neuron responses to NH_4Cl, NaCl, and NH_4I. Average percent change in RCaMP fluorescence (dF/F) over time (seconds) as described in Fig. 4. Averaged combined AFD (left and right neurons, orange) compared to left or right ASE (green) responses to (A-B) 250mM NH_4Cl (C-D) 25mM NH_4Cl (E-F) 250mM NaCl (G-H) 25mM NaCl (I-J) 250mM NH_4I (K-L) 25mM NH_4I. Shaded ribbons represent 95% confidence intervals. Shaded ribbons in (J-K) have been cropped to maintain consistent y-axes across the plots, allowing for easier comparison. Sample sizes are indicated (n).

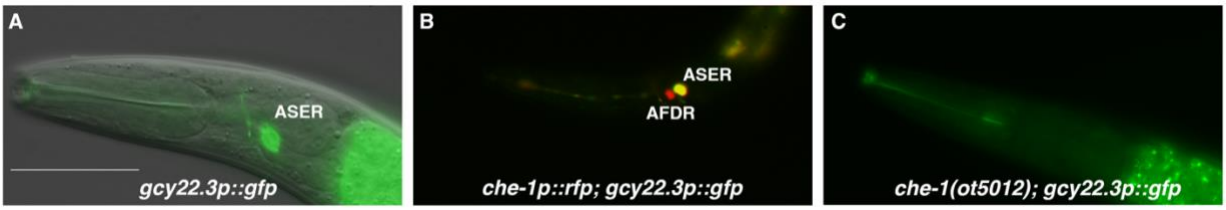

Figure 6. The laterally asymmetric expression of *gcy-22.3* is dependent on the zinc finger transcription factor CHE-1. (A) The *gcy-22.3::GFP* marker is expressed exclusively in the right ASE neuron (ASER)(n>200). (B) The *gcy-22.3::GFP* marker co-localizes with *che-1::RFP* expression in the ASER. (C) *gcy-22.3::GFP* expression is absent in the *che-1(ot5012)* mutant (n=55). Anterior is left and dorsal is top. Scale bar in (A) represents 50 µm for all panels.

653

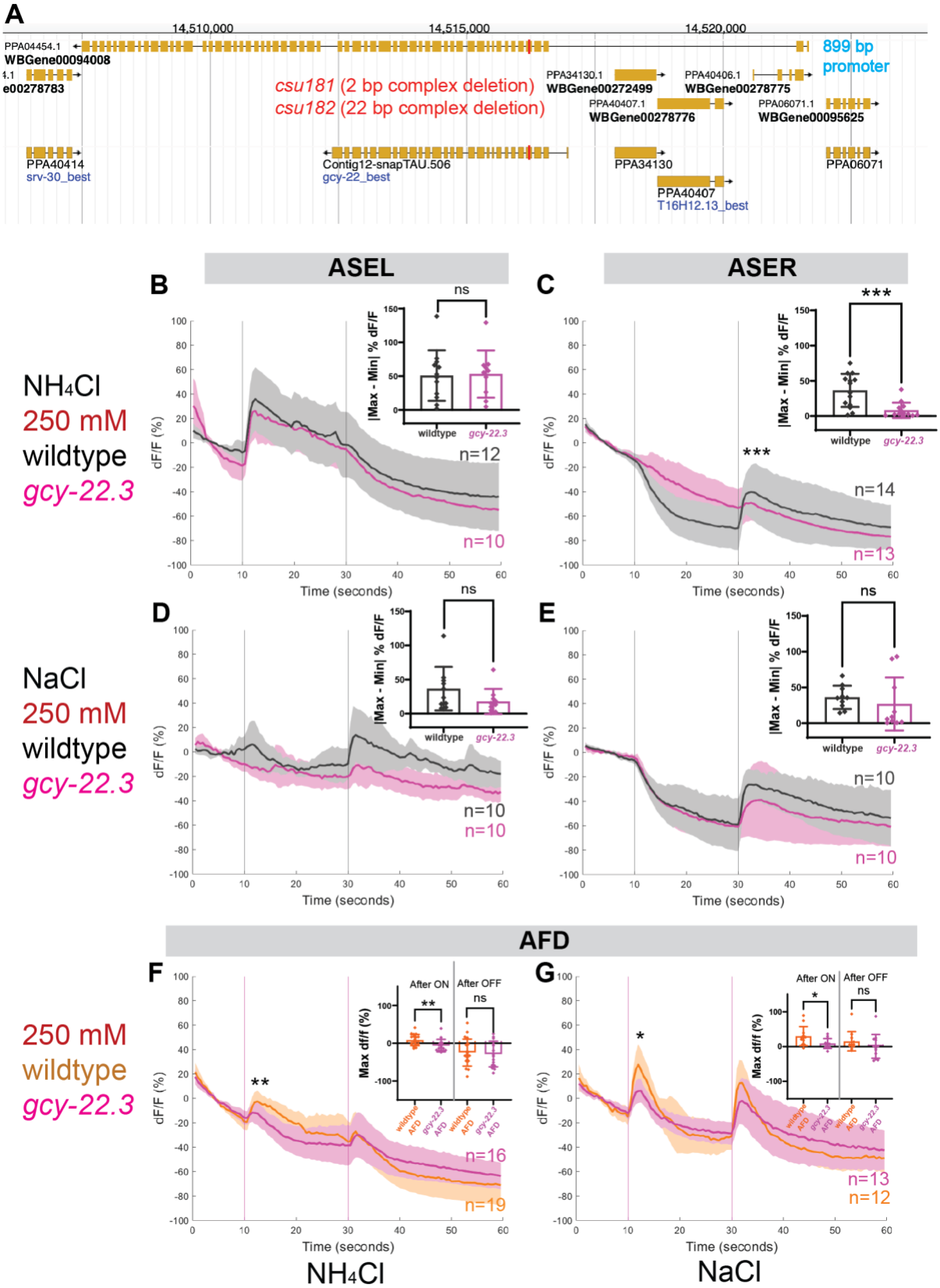
A
14,510,000
14,515,000
14,520,000
PPA04454.1
WBGene00094008
899 bp promoter
csu181 (2 bp complex deletion)
csu182 (22 bp complex deletion)
PPA34130.1
WBGene00272499
PPA40406.1
WBGene00278775
PPA40407.1
WBGene00278776
PPA06071.1
WBGene00095625
PPA40414
srv-30_best
Contig12-snapTAU.506
gcy-22_best
PPA34130
PPA06071
PPA40407
T16H12.13_best
ASEL
ASER
B
C
D
E
F
G
NH4Cl
250 mM
wildtype
gcy-22.3
NaCl
250 mM
wildtype
gcy-22.3
250 mM
wildtype
gcy-22.3
AFD
cF/F (%)
Time (seconds)
|Max - Min| % dF/F
Max df/f (%)
wildtype
gcy-22.3
After ON
After OFF
ns
n=12
n=10
n=14
n=13
n=10
n=10
n=10
n=10
n=16
n=19
n=13
n=12
NH4Cl
NaCl

654

Figure 7. ASE and AFD responses in wildtype compared to *gcy-22.3* mutants. Average percent change in RCaMP fluorescence (dF/F) over time (seconds) as described in Fig. 4. (A) www.pristionchus.org Genome Browser view of the *gcy-22.3* locus with the CRISPR/Cas9-induced mutations indicated with a red bar (Exon 5 of PPA04454 or Exon 4 of Contig12-snapTAU.506). (B-C) ASEL and ASER neuron responses to 250 mM NH_4Cl wildtype (gray) and *gcy-22.3* mutants (magenta). (D-E) ASEL and ASER neuron responses to 250 mM NaCl in wildtype (gray) and *gcy-22.3* mutants (magenta). AFD (combined left and right neurons) responses (F) to 250 mM NH_4Cl and (G) to 250 mM NaCl in wildtype (orange) and *gcy-22.3* mutants (magenta). Shaded ribbons represent 95% confidence intervals. Sample sizes are indicated (n). For ASEL/R comparisons, bar plots represent the difference between the minimum % dF/F value 10s pre-stimulus and maximum % dF/F value 10s post-stimulus for either the (B) ON or (C-E) OFF stimulus. For AFD comparisons, bar plots represent maximum % dF/F values 10s after the ON and OFF stimulus. *P<0.05, **P<0.01, ***P<0.001 indicate significant difference. “ns” indicate no significant difference. Comparisons between different genotypes were analyzed using unpaired t-test or Mann-Whitney test.

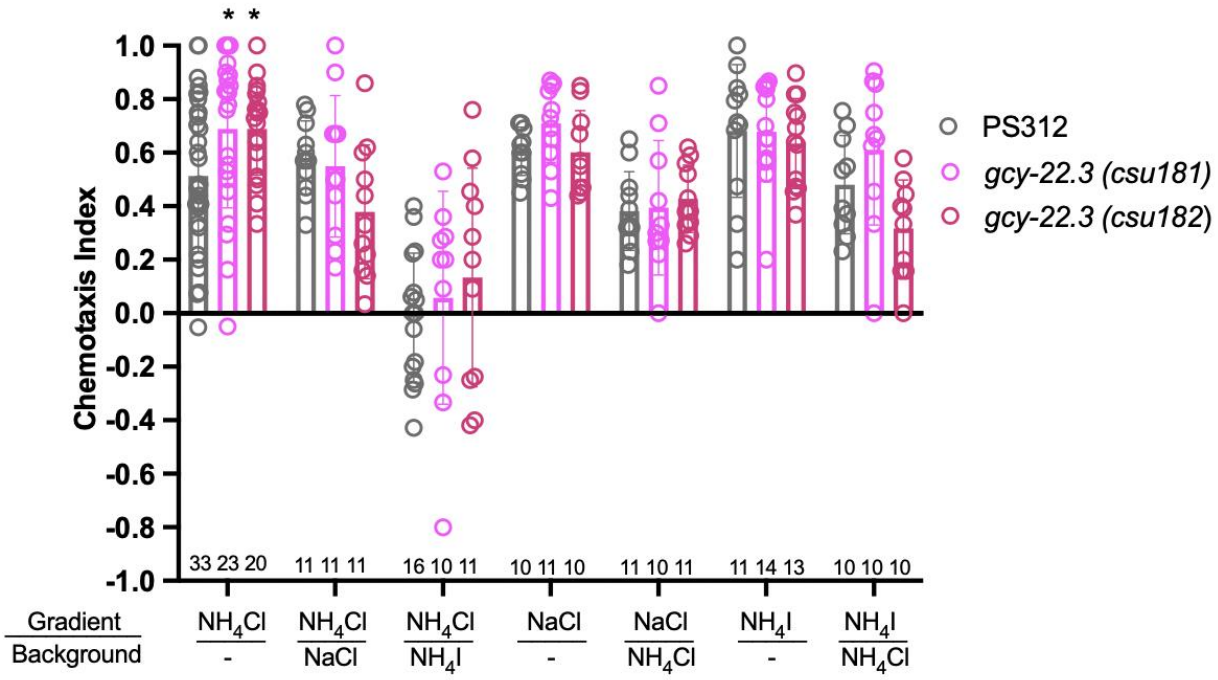

Figure 8. Chemotaxis responses to individual ions in *gcy-22.3* mutants. Young adult hermaphrodite responses to salt gradients with or without various salts in background. *P<0.05 Significant differences were found between wildtype PS312 and *gcy-22.3* mutants to NH_4Cl by two-way ANOVA and Dunnett's test. Each assay involves a minimum of 10 animals. Sample sizes for each condition are indicated on the bottom. Error bars denote standard error of the mean.

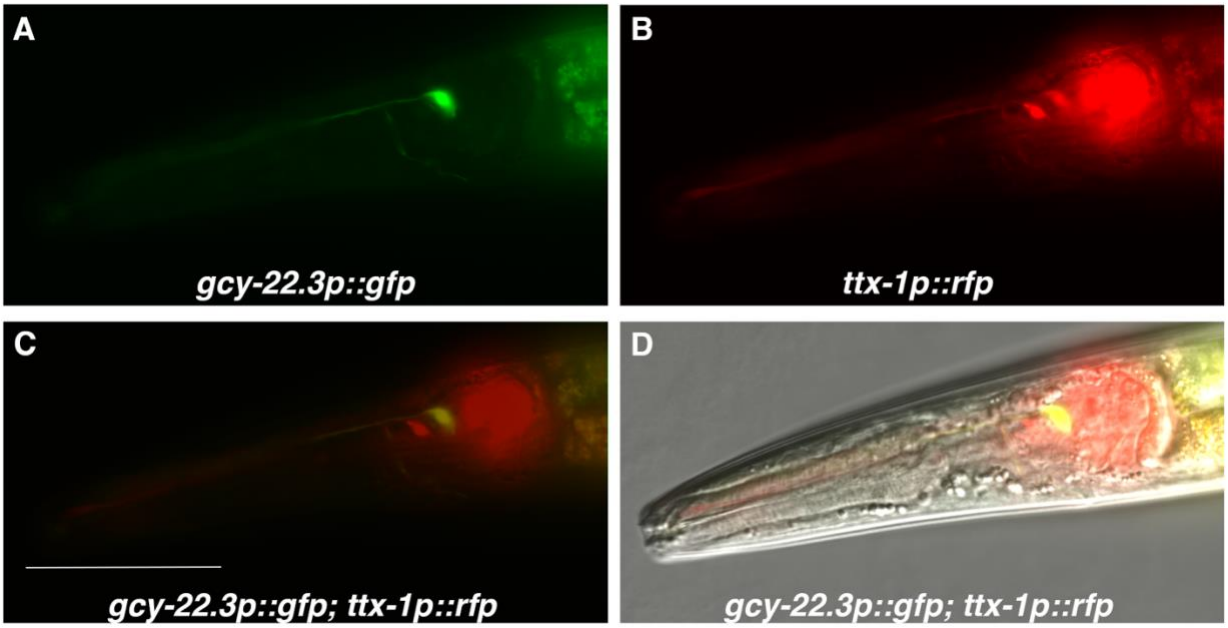

Figure S1. Co-expression of *gcy-22.3p::GFP* and *ttx-1p::RFP* in ASER. A representative F_1 male animal from a cross between the two reporter strains (n=5). Scale bar in (C) represents 50 µm for all panels.

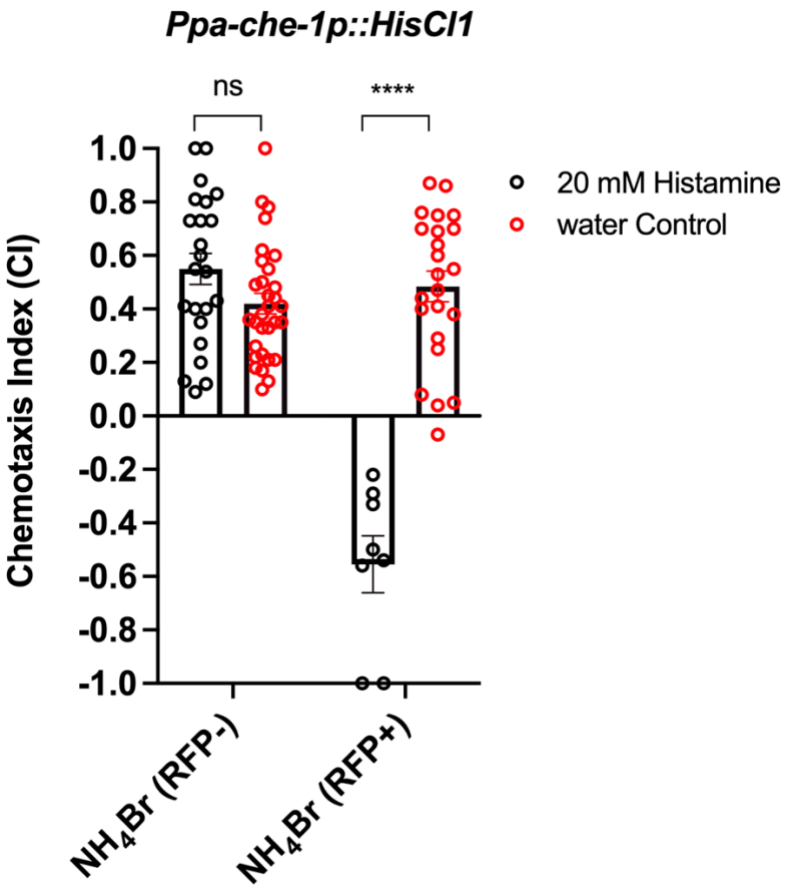

Figure S2. The *che-1p::HisCl1* transgene is necessary for histamine-dependent knockdown of salt attraction. Animals containing the *che-1p::HisCl1* transgene and the co-injection marker *egl-20p::RFP* were scored separately on each assay plate. Unpaired t-test between histamine and water treatment prior to chemotaxis assays (****P<0.0001).

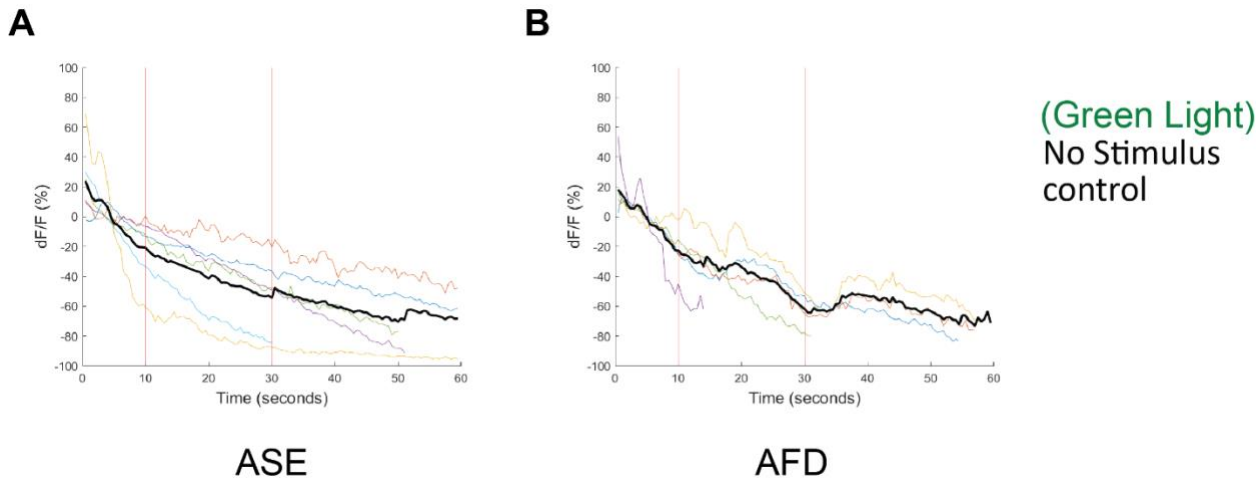

Figure S3. Negative controls of ASE and AFD neuron responses to green light. Average percent change in fluorescence (dF/F) over time (seconds) of tracked sensory neurons in *P. pacificus* (black line). Individual animals are represented by colored lines. No salt was presented; vertical lines indicate time points where salt was presented and removed for experimental samples, shown for comparison. c*suEx93[Ppa-che-1p::optRCaMP]* worms experienced the control solution for the duration of the recording and were imaged under green light. (A) ASE (n=6). (B) AFD (n=5).

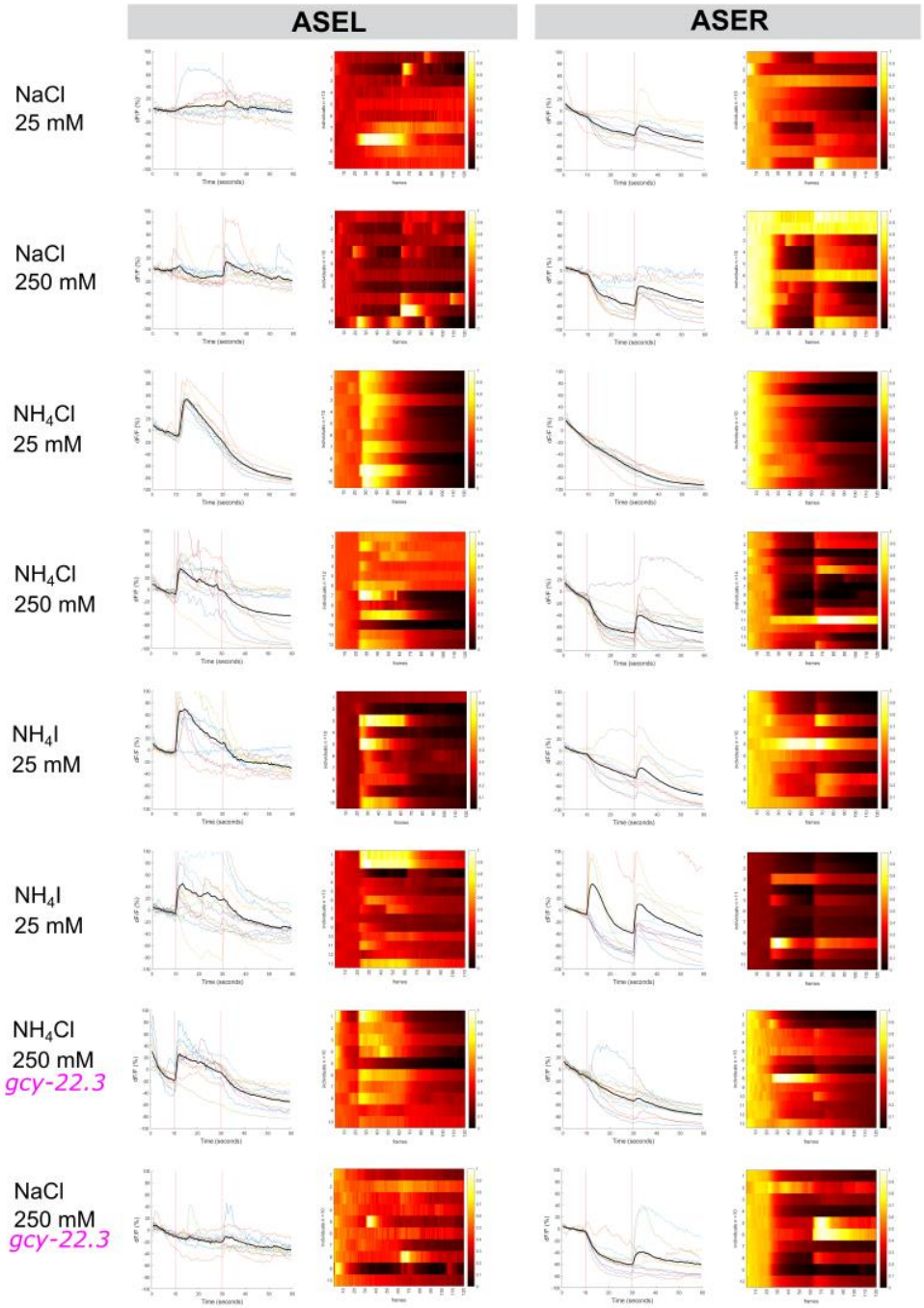

Figure S4. Individual traces and heatmaps of ASE responses to various salts. Average percent change in fluorescence (dF/F) over time (seconds) of tracked ASEL and ASER neurons in *P. pacificus* (black line). Individual animals are represented by colored lines. For heatmaps, each row represents a single individual. Lighter colors (closer to 1) represent more positive dF/F values and darker colors (closer to 0) represent more negative dF/F values.

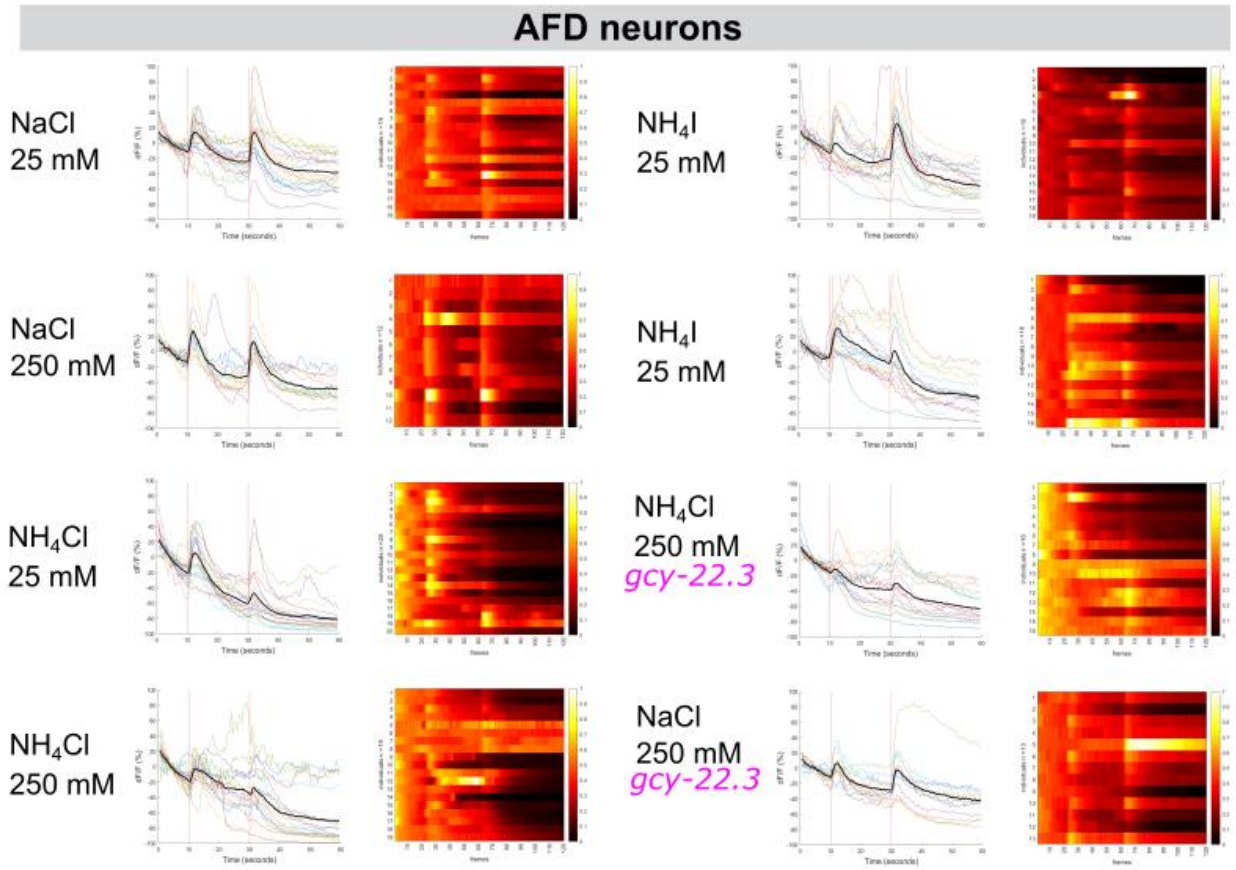

Figure S5. Individual traces and heatmaps of AFD responses to various salts. Average percent change in fluorescence (dF/F) over time (seconds) of tracked left and right AFD neurons in *P. pacificus* (black line). Individual animals are represented by colored lines. For heatmaps, each row represents a single individual. Lighter colors (closer to 1) represent more positive dF/F values and darker colors (closer to 0) represent more negative dF/F values.

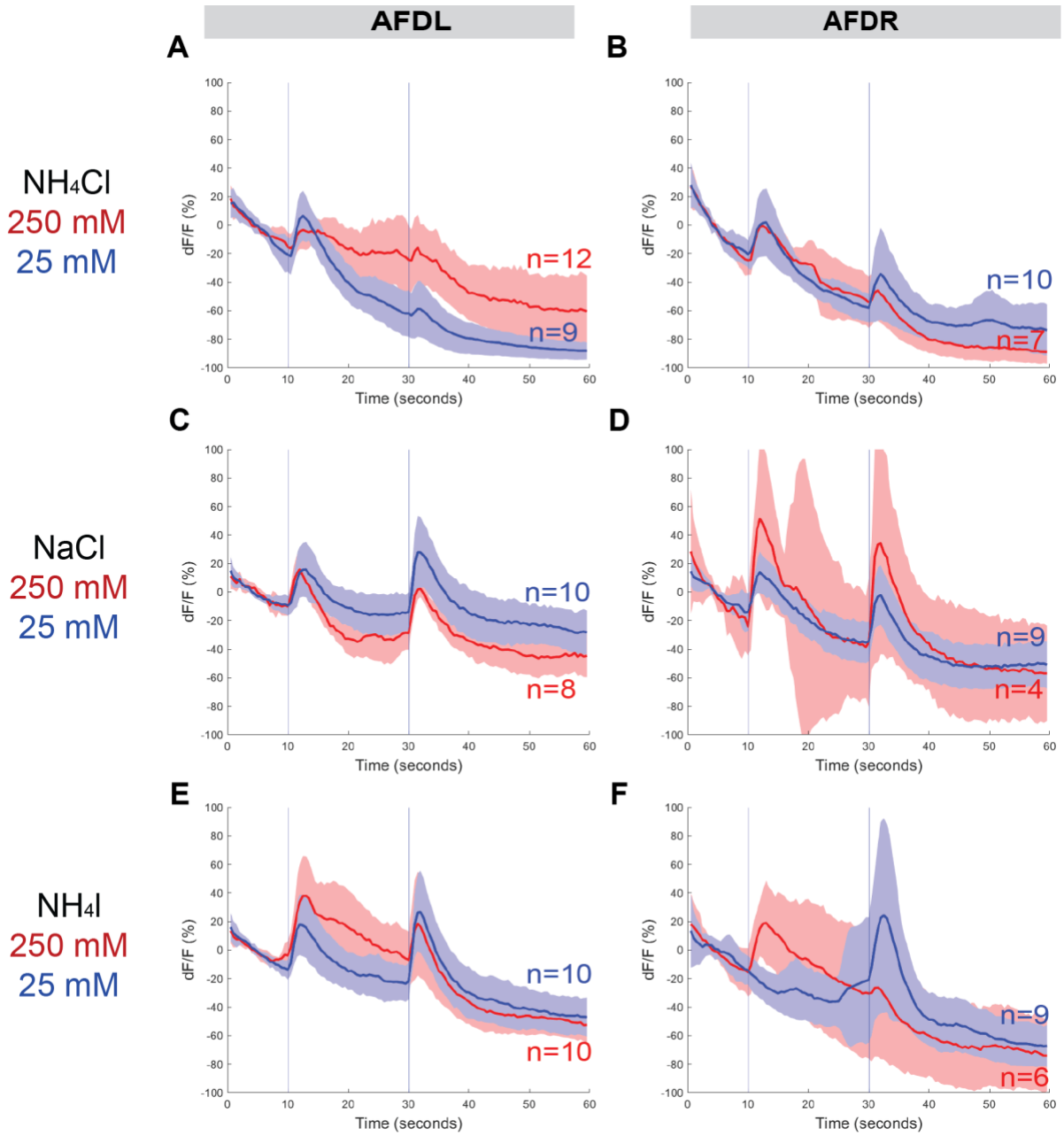

Figure S6. AFDL/R responses to different concentrations of NH_4Cl, NaCl, and NH_4I. Average percent change in RCaMP fluorescence (dF/F) over time (seconds) as described in Fig. 4. Average AFDL and AFDR neuron responses to high (250mM, red) and low (25mM, blue) concentrations of salts: (A-B) NH_4Cl, (C-D) NaCl, (E-F) NH_4I. Shaded ribbons represent 95% confidence intervals. Shaded ribbons in (D) have been cropped to maintain consistent y-axes across the plots, allowing for easier comparison. Sample sizes are indicated (n).

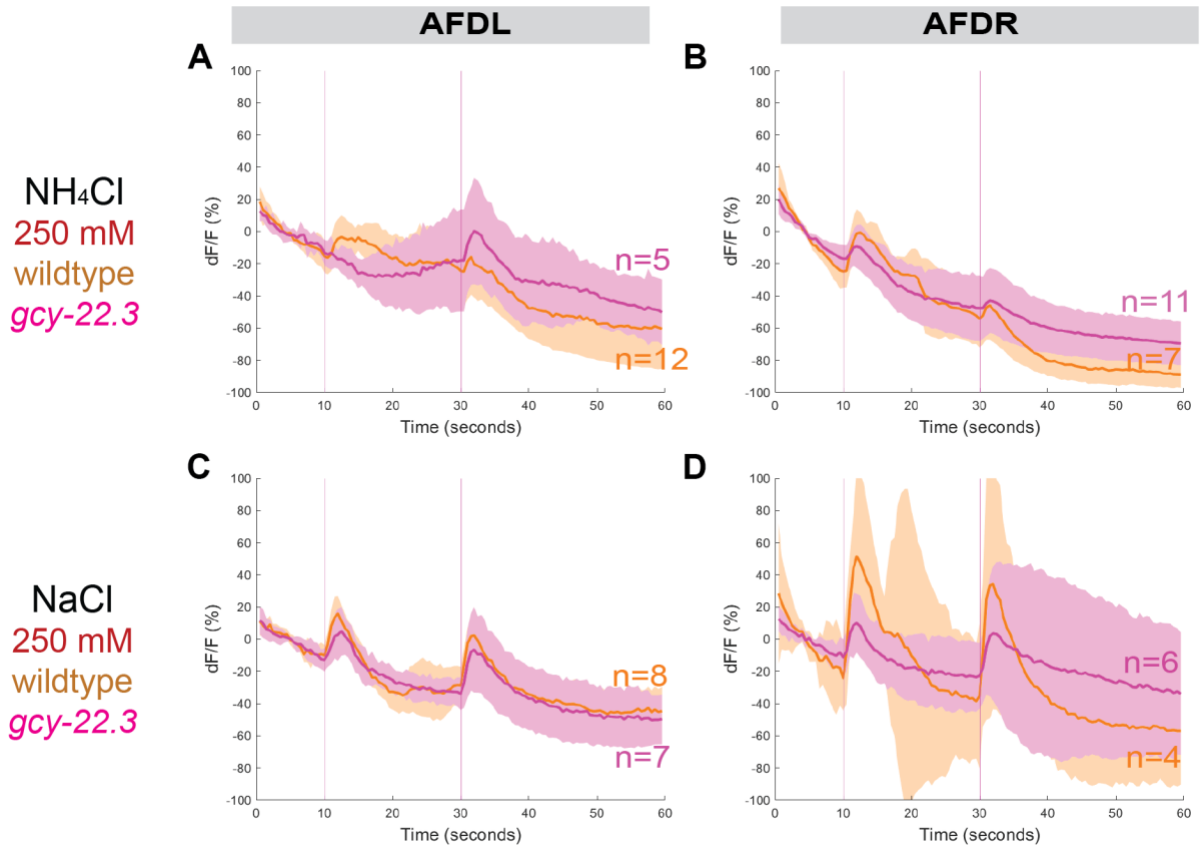

Figure S7. AFDL and AFDR responses to NH_4Cl and NaCl in wildtype and *gcy-22.3* mutant. The combined AFD responses shown in Figure 7F-7G have been separated into AFDL and AFDR. Average percent change in RCaMP fluorescence (dF/F) over time (seconds) as described in Fig. 4. AFDL and AFDR neuron responses to (A-B) 250mM NH_4Cl and (C-D) 250mM NaCl in wildtype (orange) compared to *gcy-22.3* mutants (magenta). Shaded ribbons represent 95% confidence intervals. Shaded ribbons in (D) have been cropped to maintain consistent y-axes across the plots. Sample sizes are indicated (n).

```
CHE-1(PPA01143) WT          CTACGGTCTTGGGTCGGGCTCGGCCCAGAA
ot5012 (4 bp insertion)     CTACGGTCTTGGGTCTCTGGGGCTGGCCCAGAA
ot5013 (complex indel)      CTACGGTCTTGG--AACCATAGACGAACGGGTT--CCCA


CHE-1(PPA01143) WT AA       MAYVGYDYGLG…….
ot5012 (early STOP)         MAYVG… NASDD* (frameshift +157 AA)
ot5013 (early STOP)         MAYVG… RSWTI* (frameshift +33 AA)
```

```
GCY-22.3(PPA04454) WT       AGTGACACTGGCTCAGAAATTCGAATGGACTGATCTCACCTTTATGTTCTCTGCGGAGC
csu181 (2 bp deletion)      AGTGACACTGGCTCAGAAATTCGAATGGACTGATCTCACCTTTTTTTGT--GCGGAGC
csu182 (complex indel)      AGTCCGTAGTAGTTAG----------------------CCGTAGTCCGTAGTAGTTAGC

GCY-22.3(PPA04454) WT     PIILWGPPYQSTLEDSQAFPTMMSTSFSARPRARAVVTLAQKFEWTDLTFMFSAERDPLV…   120
csu181 (early STOP).      PIILWGPPYQSTLEDSQAFPTMMSTSFSARPRARAVVTLAQKFEWTDLTFFFCGARSARW*   120
csu182 (early STOP).      PIILWGPPYQSTLEDSQAFPTMMSTSFSARPRARAVVGPVVVSRSP*                 104
```

Figure S8. Molecular lesions for *P. pacificus che-1* and *gcy-22.3*. DNA alignment of the *Ppa-che-1* and *Ppa-gcy-22.3* alleles and their predicted amino acid changes.

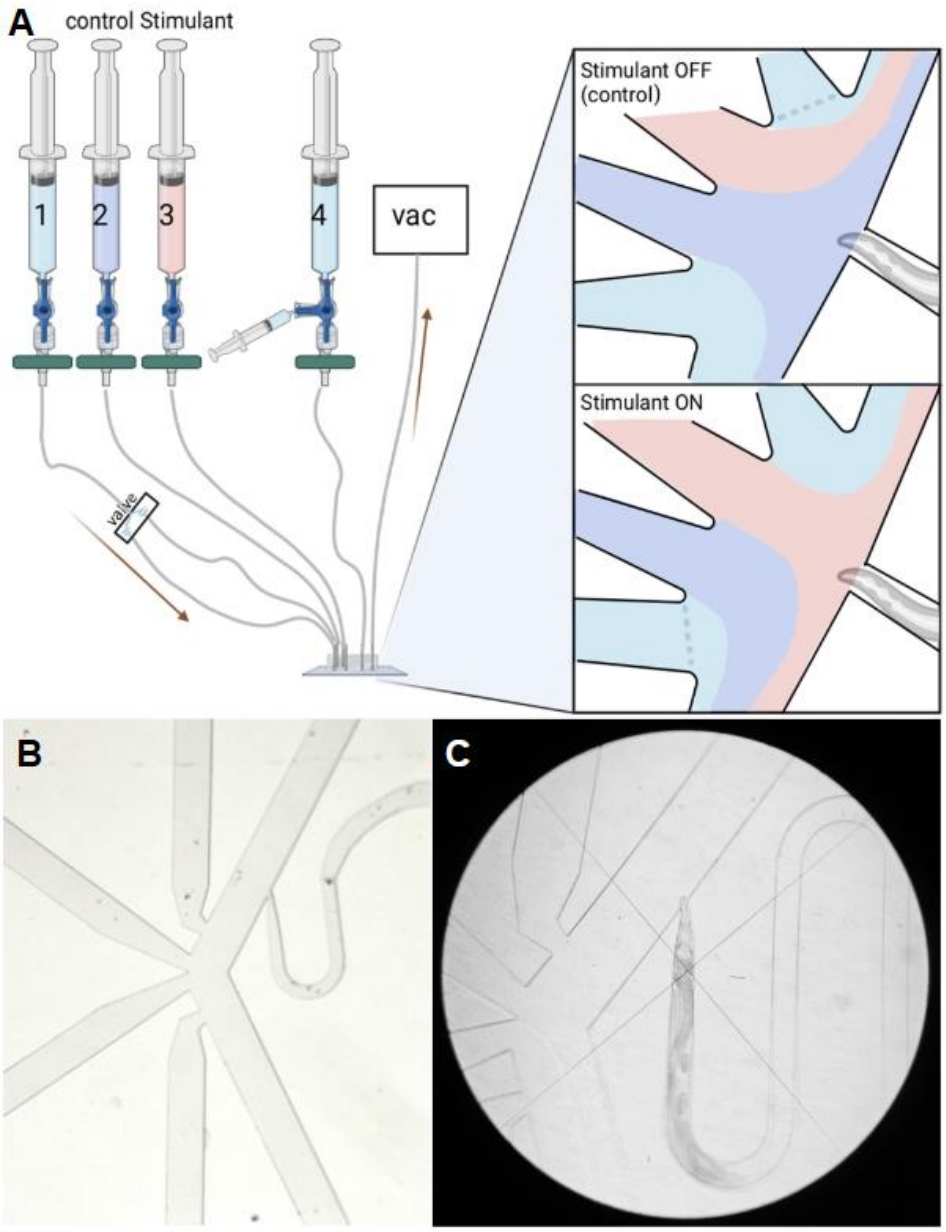

Figure S9. (A) Schematic of the microfluidic apparatus to conduct calcium imaging while delivering stimuli directly to the nose of an immobilized worm. Syringes act as reservoirs for buffer solution (light blue), control solution (purple), and stimulant solution (red). Tubing inserts into the microfluidic PDMS chip. Panels (right) zoom in to depict a schematic of the microscope view of the PDMS chip: (top) fluid flow over the worm nose when stimulant is switched OFF (control solution flows over worm nose); (bottom) fluid flow over the worm nose when stimulant is switched ON (stimulant solution flows over worm nose). Created with BioRender.com (B) Actual microscope view of PDMS chip

design. The outer two channels hold buffer solution and can be switched open (ON) or closed (OFF) by the Valvebank. The inner two channels hold experimental solutions: the inner channel closer to the worm trap holds the control solution, and the inner channel farther from the worm trap holds the stimulant solution. (C) Actual microscope view of *P. pacificus* loaded into the PDMS chip while fluid is flowing. The PDMS chip features a U-shaped worm trap to facilitate loading the worm head-first, and a tapered opening to ensure the worm fits snugly and will not slide too far forward during recording.

Table S1. Nematode strains

Gene *(Ppa-)*	**Allele**	**Strain**	**Genetic Lesion or Genotype**
--	*wildtype*	PS312	*P. pacificus* California reference strain
gcy-22.3	*csu181*	RLH293	2 bp complex deletion causing frameshift and early STOP. 2x outcrossed.
gcy-22.3	*csu182*	RLH310	22 bp complex deletion causing frameshift and early STOP. 2x outcrossed.
gcy-22.3p::GFP	*csuEx90*	RLH334	*Ppa-gcy-22.3p::GFP; Ppa-egl-20p::turboRFP*
che-1	*ot5012*	OH17879	4 bp insertion causing frameshift and STOP. 2x outcrossed.
che-1	*ot5013*	OH17880	8 bp complex indel causing frameshift and STOP. 2x outcrossed.
che-1p::HisCl1	*csuEx83*	RLH336	*Ppa-che-1pei::optHisCl1; Ppa-egl-20p::turboRFP*
che-1p::RFP	*lucEx367*	MLC545	*Ppa-che-1pei::turboRFP; Ppa-egl-20p::turboRFP*
che-1::2xALFA	*csu226*	RLH325	*Ppa-che-1::ALFA* (C-terminal tagged to last Exon)
che-1p::RCaMP; che-1p::GFP	*csuEx93*	RLH335	*Ppa-che-1pei::optRCaMP; Ppa-che-1pei::optGFP; Ppa-egl-20p::turboRFP*
che-1p::RCaMP; gcy-22.3	*csu183*	RLH300	*gcy-22.3(csu181); Ppa-che-1pei::optRCaMP; Ppa-che-1pei::optGFP; Ppa-egl-20p::turboRFP*
ttx-1p::RFP	*csuEx94*	RLH351	*Ppa-ttx-1pei::RFP (promoter with first exon and intron)*
ttx-1p::RFP	*csuEx96*	RLH352	*Ppa-ttx-1pei::RFP (promoter with first exon and intron)*
ttx-1::2xALFA	--	RLH280	*Ppa-ttx-1::ALFA* (C-terminal tagged to Exon 18)
--	*wildtype*	N2	*C. elegans* Bristol reference strain

"pei" denotes the regulatory region with promoter, exon 1, and intron 1.

Table S2. Plasmids

Plasmid	**Reporter**
pMM3	*Ppa-che-1pei::optGFP*
pMM5	*Ppa-che-1pei::optRCaMP*
pHC30	*Ppa-che-1pei::optHisCl1*
pVL2	*Ppa-gcy-22.3p::GFP*
pDC14	*Ppa-ttx-1pei::RFP*

Table S3. Primer sequences

Gene (*Ppa-*)	**Primer**	**Sequence (5'→ 3')**
che-1(PPA01143)	SJC4	CTACGGTCTTGGGTCGGGCT (crRNA, exon 1)
che-1	SJC341	ATCTCTCTCCCTCATCTCCC (forward)
che-1	SJC342	TTCCTCCCTCTCCTGACAGC (reverse)
che-1	SJC343	AGACGGATGATTAGGGAAGC (forward, nested)
che-1	SJC344	GAAGGTGTGGGAGGGTTTCC (reverse, nested)
gcy-22.3 (PPA04454)	RHL1553	TCTCACCTTTATGTTCTCTG (crRNA, exon 5)
2xALFA	ssDNA	TCTAGACTCGAGGAGGAGCTCAGAAGAAGACTCACTG AGtcCCgTctcgaggaggagctcCgTCgTCgTctcacCgag
che-1 (C-terminal ALFA)	RHL1396	CACATGAAGACGCACAAGAA (crRNA, last exon)
che-1 (C-terminal ALFA)	RHL1397	AGGTCACAAGCCTTATTCGTGC (forward)
che-1 (C-terminal ALFA)	RHL1399	GAATCTGTTGCAGCATCTGTTGC (reverse)
gcy-22.3	RHL1401	CGGTCCGGCATGCAGTCAAC (forward)
gcy-22.3	RHL1403	GTAGTCAGGCAAAGGCTCGA (reverse)
ttx-1 (C-terminal ALFA)	RHL1510	CACCGCGTAATCAATACTGC
ttx-1 (C-terminal ALFA)	RHL1511	GACCAACTACTATCCTGCAG
ttx-1 (C-terminal ALFA)	RHL1514	AGCATGGAGAACTTGGTCCA (crRNA, exon 18)

References

1. C. Bargmann, “Chemosensation in C elegans” in *WormBook*, E. Jorgensen, Ed. (2006).

2. R. L. Hong, R. J. Sommer, Chemoattraction in Pristionchus Nematodes and Implications for Insect Recognition. *Curr Biol* **16**, 2359–2365 (2006).

3. K. E. Chaisson, E. A. Hallem, Chemosensory behaviors of parasites. *Trends Parasitol* **28**, 427–436 (2012).

4. N. J. Wheeler, Z. W. Heimark, P. M. Airs, A. Mann, L. C. Bartholomay, M. Zamanian, Genetic and functional diversification of chemosensory pathway receptors in mosquito-borne filarial nematodes. *Plos Biol* **18**, e3000723 (2020).

5. S. Rengarajan, E. A. Hallem, Olfactory circuits and behaviors of nematodes. *Curr Opin Neurobiol* **41**, 136–148 (2016).

6. S. L. Koneru, H. Salinas, G. E. Flores, R. L. Hong, The bacterial community of entomophilic nematodes and host beetles. *Mol. Ecol.* **25**, 2312–2324 (2016).

7. W.-S. Lo, R. J. Sommer, Vitamin B12 and predatory behavior in nematodes. *Vitam. Horm.* **119**, 471–489 (2022).

8. W.-S. Lo, R. J. Sommer, Z. Han, Microbiota succession influences nematode physiology in a beetle microcosm ecosystem. *Nat. Commun.* **15**, 5137 (2024).

9. J. G. White, E. Southgate, J. N. Thomson, S. Brenner, The structure of the nervous system of the nematode Caenorhabditis elegans. *Philosophical Transactions Royal Soc Lond B Biological Sci* **314**, 1–340 (1986).

10. W. Schafer, Nematode nervous systems. *Curr. Biol.* **26**, R955–R959 (2016).

11. R. L. Hong, M. Riebesell, D. J. Bumbarger, S. J. Cook, H. R. Carstensen, T. Sarpolaki, L. Cochella, J. Castrejon, E. Moreno, B. Sieriebriennikov, O. Hobert, R. J. Sommer, Evolution of neuronal anatomy and circuitry in two highly divergent nematode species. *Elife* **8**, e47155 (2019).

12. S. Ward, N. Thomson, J. G. White, S. Brenner, Electron microscopical reconstruction of the anterior sensory anatomy of the nematodecaenorhabditis elegans. *J Comp Neurology* **160**, 313–337 (1975).

13. J. Li, X. Zhu, F. T. Ashton, H. R. Gamble, G. A. Schad, Sensory neuroanatomy of a passively ingested nematode parasite, Haemonchus contortus: amphidial neurons of the third-stage larva. *J Parasitol* **87**, 65–72 (2001).

14. D. J. Bumbarger, S. Wijeratne, C. Carter, J. Crum, M. H. Ellisman, J. G. Baldwin, Three-dimensional reconstruction of the amphid sensilla in the microbial feeding nematode, Acrobeles complexus (nematoda: Rhabditida). *J Comp Neurol* **512**, 271–281 (2009).

15. H. Zhu, J. Li, T. J. Nolan, G. A. Schad, J. B. Lok, Sensory neuroanatomy of Parastrongyloides trichosuri, a nematode parasite of mammals: Amphidial neurons of the first-stage larva. *J Comp Neurology* **519**, 2493–2507 (2011).

16. C. M. Loer, L. Rivard, Evolution of neuronal patterning in free-living rhabditid nematodes I: Sex-specific serotonin-containing neurons. *J Comp Neurol* **502**, 736–767 (2007).

17. T. Baiocchi, G. Lee, D.-H. Choe, A. R. Dillman, Host seeking parasitic nematodes use specific odors to assess host resources. *Sci Rep-uk* **7**, 6270 (2017).

18. S. S. Gang, M. L. Castelletto, E. Yang, F. Ruiz, T. M. Brown, A. S. Bryant, W. N. Grant, E. A. Hallem, Chemosensory mechanisms of host seeking and infectivity in skin-penetrating nematodes. *Proc. Natl. Acad. Sci.* **117**, 17913–17923 (2020).

19. A. S. Bryant, F. Ruiz, J. H. Lee, E. A. Hallem, The neural basis of heat seeking in a human-infective parasitic worm. *Curr Biol* **32**, 2206-2221.e6 (2022).

20. E. A. Hallem, A. R. Dillman, A. V. Hong, Y. Zhang, J. M. Yano, S. F. DeMarco, P. W. Sternberg, A Sensory Code for Host Seeking in Parasitic Nematodes. *Curr Biol* **21**, 377–383 (2011).

21. C. I. Bargmann, H. R. Horvitz, Chemosensory neurons with overlapping functions direct chemotaxis to multiple chemicals in C. elegans. *Neuron* **7**, 729–742 (1991).

22. Dusenbery, Sheridan, Russell, Chemotaxis Defective Mutants of the Nematode Caenorhabditis elegans. *Genetics* (1975).

23. O. Uchida, H. Nakano, M. Koga, Y. Ohshima, The C. elegans che-1 gene encodes a zinc finger transcription factor required for specification of the ASE chemosensory neurons. *Development* **130**, 1215–1224 (2003).

24. S. Chang, R. J. Johnston, O. Hobert, A transcriptional regulatory cascade that controls left/right asymmetry in chemosensory neurons of C. elegans. *Gene Dev* **17**, 2123–2137 (2003).

25. J. F. Etchberger, A. Lorch, M. C. Sleumer, R. Zapf, S. J. Jones, M. A. Marra, R. A. Holt, D. G. Moerman, O. Hobert, The molecular signature and cis-regulatory architecture of a C. elegans gustatory neuron. *Gene Dev* **21**, 1653–1674 (2007).

26. S. Yu, L. Avery, E. Baude, D. L. Garbers, Guanylyl cyclase expression in specific sensory neurons: A new family of chemosensory receptors. *Proc National Acad Sci* **94**, 3384–3387 (1997).

27. J. T. Pierce-Shimomura, S. Faumont, M. R. Gaston, B. J. Pearson, S. R. Lockery, The homeobox gene lim-6 is required for distinct chemosensory representations in C. elegans. *Nature* **410**, 694–698 (2001).

28. S. Chang, R. J. Johnston, C. Frøkjær-Jensen, S. Lockery, O. Hobert, MicroRNAs act sequentially and asymmetrically to control chemosensory laterality in the nematode. *Nature* **430**, 785–789 (2004).

29. H. Suzuki, T. R. Thiele, S. Faumont, M. Ezcurra, S. R. Lockery, W. R. Schafer, Functional asymmetry in Caenorhabditis elegans taste neurons and its computational role in chemotaxis. *Nature* **454**, 114–117 (2008).

30. C. O. Ortiz, S. Faumont, J. Takayama, H. K. Ahmed, A. D. Goldsmith, R. Pocock, K. E. McCormick, H. Kunimoto, Y. Iino, S. Lockery, O. Hobert, Lateralized Gustatory Behavior of C. elegans Is Controlled by Specific Receptor-Type Guanylyl Cyclases. *Curr Biol* **19**, 996–1004 (2009).

31. O. Hobert, Development of left/right asymmetry in the Caenorhabditis elegans nervous system: From zygote to postmitotic neuron. *genesis* **52**, 528–543 (2014).

32. R. Johnston, O. Hobert, A microRNA controlling left/right neuronal asymmetry in Caenorhabditis elegans. *Nature* **426**, 845–849 (2003).

33. L. Cochella, O. Hobert, Embryonic Priming of a miRNA Locus Predetermines Postmitotic Neuronal Left/Right Asymmetry in C. elegans. *Cell* **151**, 1229–1242 (2012).

34. R. Ahmed, Z. Chang, A. E. Younis, C. Langnick, N. Li, W. Chen, N. Brattig, C. Dieterich, Conserved miRNAs Are Candidate Post-Transcriptional Regulators of Developmental Arrest in Free-Living and Parasitic Nematodes. *Genome Biol Evol* **5**, 1246–1260 (2013).

35. S. Ward, Chemotaxis by the Nematode Caenorhabditis elegans: Identification of Attractants and Analysis of the Response by Use of Mutants. *Proc. Natl. Acad. Sci.* **70**, 817–821 (1973).

36. C. Frøkjær-Jensen, M. Ailion, S. R. Lockery, Ammonium-Acetate Is Sensed by Gustatory and Olfactory Neurons in Caenorhabditis elegans. *Plos One* **3**, e2467 (2008).

37. C. I. Bargmann, E. Hartwieg, H. R. Horvitz, Odorant-selective genes and neurons mediate olfaction in C. elegans. *Cell* **74**, 515–527 (1993).

38. J. F. Etchberger, E. B. Flowers, R. J. Poole, E. Bashllari, O. Hobert, Cis-regulatory mechanisms of left/right asymmetric neuron-subtype specification in C. elegans. *Development* **136**, 147–160 (2009).

39. C. Igreja, T. Loschko, A. Schäfer, R. Sharma, S. P. Quiobe, E. Aloshy, H. Witte, R. J. Sommer, Application of ALFA-Tagging in the Nematode Model Organisms Caenorhabditis elegans and Pristionchus pacificus. *Cells* **11**, 3875 (2022).

40. S. Kato, Y. Xu, C. E. Cho, L. F. Abbott, C. I. Bargmann, Temporal Responses of C. elegans Chemosensory Neurons Are Preserved in Behavioral Dynamics. *Neuron* **81**, 616–628 (2014).

41. W. Wang, Z.-J. Xu, Y.-Q. Wu, L.-W. Qin, Z.-Y. Li, Z.-X. Wu, Off-response in ASH neurons evoked by CuSO4 requires the TRP channel OSM-9 in Caenorhabditis elegans. *Biochem. Biophys. Res. Commun.* **461**, 463–468 (2015).

42. C. O. Ortiz, J. F. Etchberger, S. L. Posy, C. Frøkjær-Jensen, S. Lockery, B. Honig, O. Hobert, Searching for Neuronal Left/Right Asymmetry: Genomewide Analysis of Nematode Receptor-Type Guanylyl Cyclases. *Genetics* **173**, 131–149 (2006).

43. M. Herrmann, W. E. Mayer, R. L. Hong, S. Kienle, R. Minasaki, R. J. Sommer, The Nematode Pristionchus pacificus (Nematoda: Diplogastridae) Is Associated with the Oriental Beetle Exomala orientalis (Coleoptera: Scarabaeidae) in Japan. *Zool Sci* **24**, 883–889 (2007).

44. M. Herrmann, W. E. Mayer, R. J. Sommer, Sex, bugs and Haldane's rule: the nematode genus Pristionchus in the United States. *Front Zool* **3**, 14 (2006).

45. D. J. Fielding, E. Trainor, M. Zhang, Diet influences rates of carbon and nitrogen mineralization from decomposing grasshopper frass and cadavers. *Biol. Fertil. Soils* **49**, 537–544 (2013).

46. V. Piskobulu, M. Athanasouli, H. Witte, C. Feldhaus, A. Streit, R. J. Sommer, High Nutritional Conditions Influence Feeding Plasticity in Pristionchus pacificus and Render Worms Non-Predatory. *J. Exp. Zoöl. Part B: Mol. Dev. Evol.*, doi: 10.1002/jez.b.23284 (2025).

47. I. Rabinowitch, M. Chatzigeorgiou, B. Zhao, M. Treinin, W. R. Schafer, Rewiring neural circuits by the insertion of ectopic electrical synapses in transgenic C. elegans. *Nat Commun* **5**, 4442 (2014).

48. T. Shindou, M. Ochi-Shindou, T. Murayama, E. Saita, Y. Momohara, J. R. Wickens, I. N. Maruyama, Active propagation of dendritic electrical signals in C. elegans. *Sci. Rep.* **9**, 3430 (2019).

49. J. Watteyne, K. Peymen, P. V. der Auwera, C. Borghgraef, E. Vandewyer, S. V. Damme, I. Rutten, J. Lammertyn, R. Jelier, L. Schoofs, I. Beets, Neuromedin U signaling regulates retrieval of learned salt avoidance in a C. elegans gustatory circuit. *Nat. Commun.* **11**, 2076 (2020).

50. N. Chronis, M. Zimmer, C. I. Bargmann, Microfluidics for in vivo imaging of neuronal and behavioral activity in Caenorhabditis elegans. *Nat. Methods* **4**, 727–731 (2007).

51. K. Yoshida, T. Hirotsu, T. Tagawa, S. Oda, T. Wakabayashi, Y. Iino, T. Ishihara, Odour concentration-dependent olfactory preference change in C. elegans. *Nat Commun* **3**, 739 (2012).

52. I. Mori, Y. Ohshima, Neural regulation of thermotaxis in Caenorhabditis elegans. *Nature* **376**, 344–348 (1995).

53. P. Sengupta, J. H. Chou, C. I. Bargmann, odr-10 Encodes a Seven Transmembrane Domain Olfactory Receptor Required for Responses to the Odorant Diacetyl. *Cell* **84**, 899–909 (1996).

54. E. Z. Macosko, N. Pokala, E. H. Feinberg, S. H. Chalasani, R. A. Butcher, J. Clardy, C. I. Bargmann, A hub-and-spoke circuit drives pheromone attraction and social behaviour in C. elegans. *Nature* **458**, 1171–1175 (2009).

55. J. Liu, A. Ward, J. Gao, Y. Dong, N. Nishio, H. Inada, L. Kang, Y. Yu, D. Ma, T. Xu, I. Mori, Z. Xie, X. Z. S. Xu, C. elegans phototransduction requires a G protein-dependent cGMP pathway and a taste receptor homolog. *Nat. Neurosci.* **13**, 715–722 (2010).

56. S. G. Leinwand, S. H. Chalasani, Neuropeptide signaling remodels chemosensory circuit composition in Caenorhabditis elegans. *Nat. Neurosci.* **16**, 1461–1467 (2013).

57. A. Lin, S. Qin, H. Casademunt, M. Wu, W. Hung, G. Cain, N. Z. Tan, R. Valenzuela, L. Lesanpezeshki, V. Venkatachalam, C. Pehlevan, M. Zhen, A. D. T. Samuel, Functional imaging and quantification of multineuronal olfactory responses in C. elegans. *Sci Adv* **9**, eade1249 (2023).

58. E. Yemini, A. Lin, A. Nejatbakhsh, E. Varol, R. Sun, G. E. Mena, A. D. T. Samuel, L. Paninski, V. Venkatachalam, O. Hobert, NeuroPAL: A Multicolor Atlas for Whole-Brain Neuronal Identification in C. elegans. *Cell* **184**, 272-288.e11 (2021).

59. A. Zaslaver, I. Liani, O. Shtangel, S. Ginzburg, L. Yee, P. W. Sternberg, Hierarchical sparse coding in the sensory system of Caenorhabditis elegans. *Proc. Natl. Acad. Sci.* **112**, 1185–1189 (2015).

60. A. Kuhara, M. Okumura, T. Kimata, Y. Tanizawa, R. Takano, K. D. Kimura, H. Inada, K. Matsumoto, I. Mori, Temperature Sensing by an Olfactory Neuron in a Circuit Controlling Behavior of C. elegans. *Science* **320**, 803–807 (2008).

61. M. Leaver, S. Kienle, M. L. Begasse, R. J. Sommer, A. A. Hyman, A locus in Pristionchus pacificus that is responsible for the ability to give rise to fertile offspring at higher temperatures. *Biol Open* **5**, 1111–1117 (2016).

62. B. Sieriebriennikov, G. V. Markov, H. Witte, R. J. Sommer, The Role of DAF-21/Hsp90 in Mouth-Form Plasticity in Pristionchus pacificus. *Mol Biol Evol* **34**, 1644–1653 (2017).

63. M. Leaver, E. Moreno, M. Kayhan, A. McGaughran, C. Rödelsperger, R. J. Sommer, A. A. Hyman, Adaptation to environmental temperature in divergent clades of the nematode Pristionchus pacificus. *Evolution* **76**, 1660–1673 (2022).

64. J. Q. White, T. J. Nicholas, J. Gritton, L. Truong, E. R. Davidson, E. M. Jorgensen, The Sensory Circuitry for Sexual Attraction in C. elegans Males. *Curr. Biol.* **17**, 1847–1857 (2007).

65. R. J. Johnston, S. Chang, J. F. Etchberger, C. O. Ortiz, O. Hobert, MicroRNAs acting in a double-negative feedback loop to control a neuronal cell fate decision. *Proc National Acad Sci* **102**, 12449–12454 (2005).

66. D. R. Sharma, W. Röseler, H. Witte, M. S. Werner, R. J. Sommer, Developmental small RNA transcriptomics reveals divergent evolution of the conserved microRNA miR-100 and the let-7-complex in nematodes. *bioRxiv*, 2024.07.19.604269 (2024).

67. J. K. Cinkornpumin, D. R. Wisidagama, V. Rapoport, J. L. Go, C. Dieterich, X. Wang, R. J. Sommer, R. L. Hong, A host beetle pheromone regulates development and behavior in the nematode Pristionchus pacificus. *Elife* **3**, e03229 (2014).

68. S. Brenner, The Genetics of Caenorhabditis elegans. *Genetics* **77**, 71–94 (1974).

69. N. Pokala, Q. Liu, A. Gordus, C. I. Bargmann, Inducible and titratable silencing of Caenorhabditis elegans neurons in vivo with histamine-gated chloride channels. *Proc National Acad Sci* **111**, 2770–2775 (2014).

70. N. Pokala, S. W. Flavell, C. elegans, Methods and Applications. *Methods Mol Biology* **2468**, 357–373 (2022).

71. A. S. Bryant, E. A. Hallem, The Wild Worm Codon Adapter: a web tool for automated codon adaptation of transgenes for expression in non-Caenorhabditis nematodes. *G3: GenesGenomesGenet.* **11**, jkab146 (2021).

72. R. Kerr, V. Lev-Ram, G. Baird, P. Vincent, R. Y. Tsien, W. R. Schafer, Optical Imaging of Calcium Transients in Neurons and Pharyngeal Muscle of C. elegans. *Neuron* **26**, 583–594 (2000).

73. J. Nakai, M. Ohkura, K. Imoto, A high signal-to-noise Ca2+ probe composed of a single green fluorescent protein. *Nat. Biotechnol.* **19**, 137–141 (2001).

74. H. Dana, B. Mohar, Y. Sun, S. Narayan, A. Gordus, J. P. Hasseman, G. Tsegaye, G. T. Holt, A. Hu, D. Walpita, R. Patel, J. J. Macklin, C. I. Bargmann, M. B. Ahrens, E. R. Schreiter, V. Jayaraman, L. L. Looger, K. Svoboda, D. S. Kim, Sensitive red protein calcium indicators for imaging neural activity. *eLife* **5**, e12727 (2016).

75. Z. Han, W.-S. Lo, J. W. Lightfoot, H. Witte, S. Sun, R. J. Sommer, Improving Transgenesis Efficiency and CRISPR-Associated Tools Through Codon Optimization and Native Intron Addition in Pristionchus Nematodes. *Genetics* **216**, genetics.303785.2020 (2020).

76. K. Nakayama, Y. Ishita, T. Chihara, M. Okumura, Screening for CRISPR/Cas9-induced mutations using a co-injection marker in the nematode Pristionchus pacificus. *Dev Genes Evol*, 1–8 (2020).

77. S. H. Chalasani, N. Chronis, M. Tsunozaki, J. M. Gray, D. Ramot, M. B. Goodman, C. I. Bargmann, Dissecting a circuit for olfactory behaviour in Caenorhabditis elegans. *Nature* **450**, 63–70 (2007).

78. T. Stiernagle, Maintenance of C. elegans. *WormBook : online Rev. C elegans Biol.*, 1–11 (2006).

79. Z. Liu, M. J. Kariya, C. D. Chute, A. K. Pribadi, S. G. Leinwand, A. Tong, K. P. Curran, N. Bose, F. C. Schroeder, J. Srinivasan, S. H. Chalasani, Predator-secreted sulfolipids induce defensive responses in C. elegans. *Nat Commun* **9**, 1128 (2018).

Acknowledgement

This research is funded by NIH SC1GM140970 to RLH, NIH R56MH096881 to SHC. OH is funded by the HHMI. MM and RLH contributed in conception, design and acquisition of work. VL, HRC, DLC, IMD, NRK, KTQ, and SJC contributed to data acquisition. RLH, OH, and SHC contributed to the analysis and writing of the work. The authors declare that they have no competing interests. We would also like to thank I. Martinez and C. Igreja for technical assistance, and M. Barsegyan for assistance with data acquisition. All data needed to evaluate the conclusions in the paper are present in the paper and the Supplementary Materials.